Interferometry of non-Abelian Anyons

Parsa Bonderson [a,c,*], Kirill Shtengel [b,c], J. K. Slingerland [b,c]

[a] *Microsoft Research, Station Q, CNSI Building, University of California, Santa Barbara, CA 93106, USA*

[b] *Department of Physics and Astronomy, University of California, Riverside, CA 92521, USA*

[c] *California Institute of Technology, Pasadena, CA 91125, USA*

Abstract

We develop the general quantum measurement theory of non-Abelian anyons through interference experiments. The paper starts with a terse introduction to the theory of anyon models, focusing on the basic formalism necessary to apply standard quantum measurement theory to such systems. This is then applied to give a detailed analysis of anyonic charge measurements using a Mach-Zehnder interferometer for arbitrary anyon models. We find that, as anyonic probes are sent through the legs of the interferometer, superpositions of the total anyonic charge located in the target region collapse when they are distinguishable via monodromy with the probe anyons, which also determines the rate of collapse. We give estimates on the number of probes needed to obtain a desired confidence level for the measurement outcome distinguishing between charges, and explicitly work out a number of examples for some significant anyon models. We apply the same techniques to describe interferometry measurements in a double point-contact interferometer realized in fractional quantum Hall systems. To lowest order in tunneling, these results essentially match those from the Mach-Zehnder interferometer, but we also provide the corrections due to processes involving multiple tunnelings. Finally, we give explicit predictions describing state measurements for experiments in the Abelian hierarchy states, the non-Abelian Moore-Read state at $\nu = 5/2$ and Read-Rezayi state at $\nu = 12/5$.

Key words: Non-Abelian Anyons; Interferometry; Anyonic charge measurement; Fractional quantum Hall effect; Topological qubit readout.
PACS: 03.65.Ta, 03.65.Vf, 05.30.Pr, 73.43.-f

* Corresponding author.
Email addresses: parsab@microsoft.com (Parsa Bonderson), kirill.shtengel@ucr.edu (Kirill Shtengel), joost.slingerland@gmail.com (J. K. Slingerland).

1 Introduction

One of the striking differences between two and three spatial dimensions is manifested in the allowed exchange statistics of quantum particles. In three spatial dimensions, the allowed particle types can be classified according to irreducible representations of the permutation group. There are only two such one-dimensional representations, the trivial and alternating representations, for which exchange of any two particles introduces a factor of 1 and -1, respectively, to the wavefunction, corresponding to bosonic and fermionic statistics. Multi-dimensional representations of the permutation group give rise to what is known as "parastatistics" [1], however, it has been shown that parastatistics can be replaced by bosonic and fermionic statistics, if a hidden degree of freedom (a non-Abelian isospin group) is introduced [2].

In contrast, for two spatial dimensions the particles are classified according to representations of the braid group [3]. The corresponding types of particles have been dubbed "anyons" [4,5], and their exchange statistics are more precisely referred to as "braiding statistics." Braiding statistics described by multi-dimensional irreducible representations of the braid group [6] give rise to non-Abelian anyons. [1]

The group representation theory used to characterize particles' braiding statistics, however, becomes progressively cumbersome if one attempts to describe a system with several distinct "species" of anyons, especially those corresponding to multi-dimensional representations. Furthermore, one would typically like to consider systems in which there are processes that do not conserve particle number, a notion unsupported by the group theoretic language. To circumvent these shortcomings for systems with two spatial dimensions, one may switch over to the quantum field theoretic-type formalism of anyon models, in which the topological and algebraic properties of the anyonic system are described by category theory, rather than group theory. The structures of anyon models originated from conformal field theory (CFT) [7,8] and Chern-Simons theory [9]. They were further developed in terms of algebraic quantum field theory [10,11], and made mathematically rigorous in the language of braided tensor categories [12,13,14].

Surprisingly, even in our three-dimensional universe, there are physical systems that are *effectively* two dimensional and have quasiparticles – point-like localized coherent state excitations that behave like particles – that appear to possess such exotic braiding statistics. In fact, some of these are even strongly believed (though, thus far, experimentally unconfirmed) to be non-Abelian anyons. Anyon models describe the topological behavior of quasiparticle excitations in two-dimensional, many-body systems with an energy gap that suppresses (non-topological) long-range interactions, and hence an anyon model is said to characterize a system's

[1] In this paper, the term "anyon" will be used in reference to both the Abelian and non-Abelian varieties.

"topological order."

The fractional quantum Hall effect is the most prominent example of anyonic systems, so we will briefly review some relevant facts on the subject. (For a general introduction into the quantum Hall effect we refer the reader to Refs. [15,16,17,18].) The quantum Hall effect is an anomalous Hall effect that occurs in two dimensional electron gases (2DEGs) subjected to strong transverse magnetic fields (~ 10 T) at very low temperatures (~ 10 mK). Under these conditions, the Hall resistance R_{xy} develops plateaus while R_{xx} develops a series of deep minima as a function of the applied magnetic field. These plateaus occur at values which are quantized to extreme precision in integer [19] or fractional [20] multiples of the fundamental conductance quantum e^2/h. These multiples are the filling fractions, usually denoted $\nu \equiv N_{\rm e}/N_\phi$ where $N_{\rm e}$ is the number of electrons and N_ϕ is the number of fundamental flux quanta through the area occupied by the 2DEG at magnetic field corresponding to the center of a plateau. At the plateaus, the conductance tensor is off-diagonal, meaning a dissipationless transverse current flows in response to an applied electric field. In particular, the electric field generated by threading an additional localized flux quantum through the system expels a net charge of νe, thus creating a quasihole. Consequently, charge and flux are intimately coupled together in the quantum Hall effect.

In the fractional quantum Hall (FQH) regime, electrons form an incompressible fluid state that supports localized excitations (quasiholes and quasiparticles) which, for the simplest cases, carry one magnetic flux quantum and, hence, fractional charge νe. This combination of fractional charge and unit flux implies that they are anyons, due to their mutual Aharonov–Bohm effect. The fractional charge of quasiparticles in the $\nu = 1/3$ Laughlin state was first measured in 1995 [21]. Recently, a series of experiments asserting verification of the fractional braiding statistics has been reported [22,23,24,25,26,27].

In the bulk of a FQH sample, the long-distance interactions between quasiholes are purely topological and may be described by an anyon model. Boundary excitations and currents of the Hall liquid are described by a $1+1$ dimensional conformal field theory [28] whose topological order is the same as that of the bulk, when there is no edge reconstruction [29,30]. These boundary excitations provide one way of coupling measurement devices to the 2DEG. A further connection between the physics of the bulk and CFT can be established following the observation in [31] that the microscopic trial wavefunction describing the ground state of the incompressible FQH liquid can be constructed from conformal blocks (CFT correlators).

For the purpose of this paper, we are particularly interested in the possibility of non-Abelian statistics existing at several observed plateaus in the second Landau level ($2 \leq \nu \leq 4$), in particular $\nu = 5/2$, $7/2$, and $12/5$ [32,33,34,35]. Predictions of non-Abelian statistics in FQH states originated with the paired state of Moore and Read [31], and was generalized by Read and Rezayi to a series of clustered non-

Abelian states [36]. At least for $\nu = 5/2$ (the Moore–Read state) and $\nu = 12/5$ (the $k = 3, M = 1$ Read–Rezayi state), these wavefunctions were found to have very good overlap with the exact ground states obtained by numerical diagonalization of small systems [37,38].

Detailed investigations of the braiding behavior of quasiholes of the Moore–Read state were carried out in Ref. [39], and of the $\nu = 12/5$ state, as well as the other states in the Read–Rezayi series in Ref. [40]. Owing to the special feature of the Moore–Read state as a weakly-paired state of a $p + \mathrm{i}p$ superconductor of composite fermions [41], alternative explicit calculations of the non-Abelian exchange statistics of quasiparticles were carried out in the language of unpaired, zero-energy Majorana modes associated with the vortex cores [42,43]. (Unfortunately, this language does not readily adapt to give a similar interpretation for the other states in the Read–Rezayi series.)

In addition to the proposed fractional quantum Hall states that could host non-Abelian anyons [31,36,44], there are a number of other more speculative proposals of systems that may be able to exhibit non-Abelian braiding statistics. These include lattice models [45,46], quantum loop gases [47,48,49,50], string-net gases [51,52,53,54], Josephson junction arrays [55], $p + \mathrm{i}p$ superconductors [56,57,58], and rapidly rotating bose condensates [59,60,61]. Since non-Abelian anyons are representative of an entirely new and exotic phase of matter, their discovery would be of great importance, in and of itself. However, as additional motivation, non-Abelian anyons could also turn out to be an invaluable resource for quantum computing.

The idea to use the non-local, multi-dimensional state space shared by non-Abelian anyons as a place to encode qubits was put forth by Kitaev [45], and further developed in Refs. [62,63,64,65,66,67,68]. The advantage of this scheme, known as "topological quantum computing," is that the non-local state space is impervious to local perturbations, so the qubit encoded there is "topologically" protected from errors. A model for topological qubits in the Moore–Read state was proposed in Ref. [69], however braiding operations alone in this state are not computationally universal, severely limiting its usefulness in this regard. Nevertheless, one may still hope to salvage the situation by supplementing braiding in the Moore–Read state with topology changing operations [70,71] or non-topologically protected operations [72] to produce universality. The greater hope, however, lies in the $k = 3$ Read–Rezayi state, for which the non-Abelian braiding statistics are essentially described by the computationally universal "Fibonnaci" anyon model (see Section 3.6.2). Consequently, the efforts in "topological quantum compiling" (i.e. designing anyon braids that produce desired computational gates) for this anyon model [73,74,75] may be applied directly.

The primary focus of this paper is to address the measurement theory of anyonic charge. This provides a key element in detecting non-Abelian statistics and cor-

rectly identifying the topological order of a system. Furthermore, the ability to perform measurements of anyonic charge is a crucial component of topological quantum computing, in particular for the purposes of qubit initialization and readout. Clearly, the most direct way of probing braiding statistics is through experiments that establish interference between different braiding operations. In this vein, we will consider interferometry experiments which probe braiding statistics via Aharonov–Bohm type interactions [76], where probe anyons exhibit quantum interference between homotopically distinct paths traveled around a target, producing measurement distributions that distinguish different anyonic charges in the target. This sort of experiment provides a quantum non-demolitional measurement [77] and is ideally suited for the qubit readout procedure in topological quantum computing.

The paper is structured as follows:

In Section 2, we provide an introduction to the theory of anyon models, giving all the essential background needed to understand the rest of the paper, and establishing the connection with standard concepts of quantum information theory.

In Section 3, we analyze a Mach-Zehnder type interferometer for an arbitrary anyon model. We consider a target anyon allowed to be in a superposition of anyonic states, and describe its collapse behavior resulting from interferometry measurements by probe anyons. We find that probe anyons will collapse any superpositions of states they can distinguish by monodromy, as well as decohere anyonic charge entanglement that they can detect between the target and outside anyons. We show how these measurements may be used to determine the target's anyonic charge and/or help identify the topological order of a system. We conclude this section by applying the results to a few particularly relevant examples.

In Section 4, we consider a double point-contact interferometer designed for fractional quantum Hall systems. We give the evolution operator to all orders in tunneling, and apply the methods and results of Section 3 to describe how superpositions in the target anyon state collapse as a result of interferometry measurements, and how to determine the anyonic charge of the target. We give detailed predictions for the Abelian hierarchy states, the Moore–Read state ($\nu = 5/2, 7/2$), and the $k = 3, M = 1$ Read–Rezayi state ($\nu = 12/5$).

2 Anyon Models

In this section, we briefly review aspects of the theory of anyon models which are relevant to the rest of the paper. We follow the relatively concrete approach found in Refs. [46,78], and develop some concepts in this formalism that are essential for the treatment of the measurement problem, such as the density matrix description

of states and the partial trace and partial quantum trace.

2.1 Fusion and Quantum Dimensions

An anyon model has a finite set $\mathcal{C}$ of superselection sector labels called topological or anyonic charges. These conserved charges obey a commutative, associative fusion algebra

$$a \times b = \sum_{c \in \mathcal{C}} N_{ab}^{c} c \tag{2.1}$$

where the fusion multiplicities N_{ab}^{c} are non-negative integers which indicate the number of different ways the charges a and b can be combined to produce the charge c. There is a unique trivial "vacuum" charge $1 \in \mathcal{C}$ for which $N_{a1}^{c} = \delta_{ac}$, and each charge a has a unique conjugate charge, or "antiparticle," $\bar{a} \in \mathcal{C}$ such that $N_{ab}^{1} = \delta_{b\bar{a}}$. ($1 = \bar{1}$ and $\bar{\bar{a}} = a$.)

In order to have a non-Abelian representation of the braid group (details on braiding follow), there must be at least one pair of charges a and b in the theory which have multiple fusion channels, i.e.

$$\sum_{c} N_{ab}^{c} > 1, \tag{2.2}$$

The domain of a sum will henceforth be left implicit when it runs over all possible labels. Charges a which have $\sum_c N_{ab}^{c} = 1$ for every b must correspond to Abelian anyons (possibly bosons or fermions). Abelian and non-Abelian charges may also be distinguished by their *quantum dimensions*. The quantum dimension d_a of a charge a is a measure for the amount of entropy contributed to the system by the presence of a particle of type a. It may be found from the fusion multiplicities by considering the asymptotic scaling of the number of possible fusion channels for n anyons of charge a. For large n, this scales as d_a^n. Abelian charges have quantum dimension equal to 1, while non-Abelian charges quantum dimensions strictly larger than 1. The *total quantum dimension* of an anyon model is defined as

$$\mathcal{D} = \sqrt{\sum_{a} d_a^2}. \tag{2.3}$$

2.2 States, Operators and Inner Product

To each fusion product, there is assigned a fusion vector space V_{ab}^{c} with $\dim V_{ab}^{c} = N_{ab}^{c}$, and a corresponding splitting space V_{c}^{ab}, which is the dual space. We pick some orthonormal set of basis vectors $|a, b; c, \mu\rangle \in V_{c}^{ab}$ ($\langle a, b; c, \mu| \in V_{ab}^{c}$) for these spaces, where $\mu = 1, \ldots, N_{ab}^{c}$. If $N_{ab}^{c} = 0$, then V_{c}^{ab} is zero-dimensional and it has no basis elements. We will sometimes use the notation $c \in \{a \times b\}$ to mean c such that $N_{ab}^{c} \neq 0$. Allowed splitting and fusion spaces involving the vacuum charge have dimension one, and so we will leave their basis vector labels $\mu = 1$ implicit.

It is extremely useful to employ a diagrammatic formalism for anyon models. Each anyonic charge label is associated with an oriented line. It is useful in some contexts to think of these lines as the anyons' worldlines (we will consider time as increasing in the upward direction), however, such an interpretation is not necessary nor even always appropriate. Reversing the orientation of a line is equivalent to conjugating the charge labeling it, i.e.

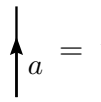

(2.4)

The fusion and splitting states are assigned to trivalent vertices with the appropriately corresponding anyonic charges:

$$(d_c/d_a d_b)^{1/4}$$ 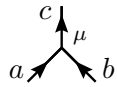

$$= \langle a, b; c, \mu| \in V_{ab}^{c}, \tag{2.5}$$

$$(d_c/d_a d_b)^{1/4}$$ 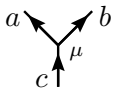

$$= |a, b; c, \mu\rangle \in V_{c}^{ab}, \tag{2.6}$$

where the normalization factors $(d_c/d_a d_b)^{1/4}$ are included so that diagrams are in the isotopy invariant convention throughout this paper. Isotopy invariance means that the value of a (labeled) diagram is not changed by continuous deformations, so long as open endpoints are held fixed and lines are not passed through each other or around open endpoints. Open endpoints should be thought of as ending on some boundary (e.g. a timeslice or an edge of the system) through which isotopy is not permitted. Building in isotopy invariance is a bit more complicated than just making this normalization change, but for the purposes of this paper, we can ignore the full details (which can be found in [46,79]).

Inner products are formed diagrammatically by stacking vertices so the fusing/splitting lines connect

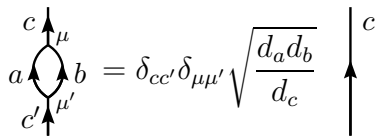

$$= \delta_{cc'}\delta_{\mu\mu'}\sqrt{\frac{d_a d_b}{d_c}} \tag{2.7}$$

and this generalizes to more complicated diagrams. An important feature of this relation is that it diagrammatically encodes charge conservation, and, in particular, forbids tadpole diagrams. An important special case is $c = 1$, which shows that an unknotted loop carrying charge a evaluates to its quantum dimension

$$= d_a = d_{\bar{a}}. \tag{2.8}$$

The completeness relation for the identity operator on a pair of anyons with charges

a and b respectively is written diagrammatically as

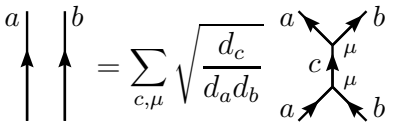

(2.9)

Any diagrammatic equation, such as this, is also valid as a local relation within larger, more complicated diagrams. Using Eq. (2.9), Eq. (2.7) and isotopy, we get the following important relation, which expresses the compatibility of the quantum dimensions with fusion.

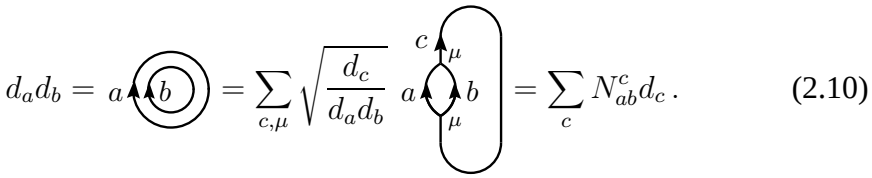

(2.10)

For general operators, we introduce the notation

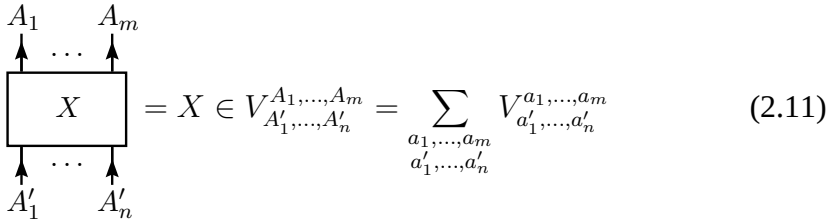

(2.11)

where a capitalized anyonic charge label means a (direct) sum over all possible charges, so that the operator X is defined for acting on any n anyon input and m anyon output. The box stands for a linear combination of diagrams describing the action of the operator. The indices on operators will be left implicit when they are contextually clear (and unnecessary). Conjugation of a diagram or operator is carried out by simultaneously reflecting the diagram across the horizontal plane and reversing the orientation of arrows.

Tensoring together two operators (on separate sets of anyons) is simply executed by juxtaposition of their diagrams:

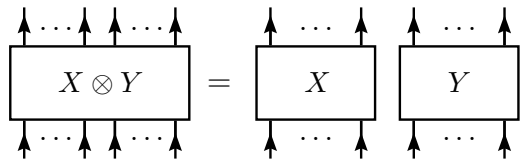

(2.12)

2.3 Associativity

The splitting of three anyons with charges a, b, c from the charge d corresponds to a space V_d^{abc} which can be decomposed into tensor products of two anyon splitting spaces by matching the intermediate charge. This can be done in two isomorphic ways

$$V_d^{abc} \cong \bigoplus_e V_e^{ab} \otimes V_d^{ec} \cong \bigoplus_f V_d^{af} \otimes V_f^{bc}. \tag{2.13}$$

To incorporate the notion of associativity at the level of splitting spaces, we need to specify a set of unitary isomorphisms between different decompositions that are to be considered simply a change of basis. These isomorphisms (called F-moves) are written diagrammatically as

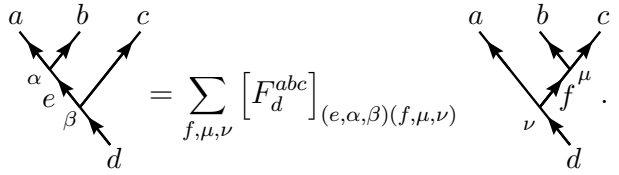

(2.14)

The same notion of associativity is, of course, true for fusion of three anyons. The associativity for fusion is given by $F^\dagger$, and together with unitarity, we have

$$\left[\left(F_d^{abc}\right)^\dagger\right]_{(f,\mu,\nu)(e,\alpha,\beta)} = \left[F_d^{abc}\right]^*_{(e,\alpha,\beta)(f,\mu,\nu)} = \left[\left(F_d^{abc}\right)^{-1}\right]_{(f,\mu,\nu)(e,\alpha,\beta)}. \tag{2.15}$$

For fusion and splitting of more anyons, one does the obvious iteration of such decompositions. For this to be consistent, the F-symbols must satisfy a constraint called the Pentagon equation. One also imposes the physical requirement that fusion and splitting with the vacuum charge does not change the state. This means in particular that in diagrams, we may move, add, and delete vacuum lines at will (in fact, we already did this in Eq. 2.8). Despite the constraints, the F-symbols have a certain amount of "gauge freedom," which comes from the fact that we are free to choose bases for the vertex spaces.

We will also need the F-move with one of its legs bent down

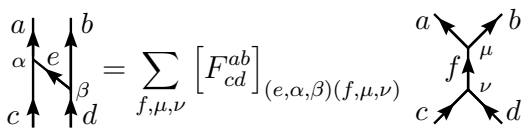

(2.16)

which is also a unitary transformation. From Eq. (2.9), we immediately find that

$$\left[F_{ab}^{ab}\right]_{1(c,\mu,\nu)} = \left[\left(F_{ab}^{ab}\right)^{-1}\right]_{(c,\mu,\nu)1} = \sqrt{\frac{d_c}{d_a d_b}}\,\delta_{\mu\nu}, \tag{2.17}$$

and more generally, applying Eqs. (2.9) and (2.7) gives a relation between the two

types of F-symbols

$$\left[F_{cd}^{ab}\right]_{(e,\alpha,\beta)(f,\mu,\nu)} = \sqrt{\frac{d_e d_f}{d_a d_d}} \left[F_f^{ceb}\right]^*_{(a,\alpha,\mu)(d,\beta,\nu)} . \tag{2.18}$$

2.4 Trace and Partial Trace

The trace over operators formed from bras and kets is defined in the usual way. To translate the trace into the diagrammatic formalism, one defines the *quantum trace*, denoted $\widetilde{\mathrm{Tr}}$, by closing the diagram with loops that match the outgoing lines with the respective incoming lines at the same position

$\widetilde{\mathrm{Tr}}X = \widetilde{\mathrm{Tr}}$ 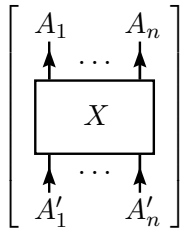

$=$ 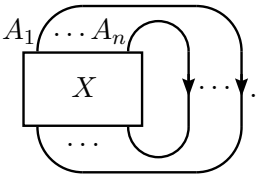

. (2.19)

Connecting the endpoints of two lines labeled by different anyonic charges violates charge conservation, so such diagrams evaluate to zero. The operator $X \in V^{A_1 \ldots A_n}_{A'_1 \ldots A'_n}$ may be written as

$$X = \sum_c X_c, \qquad X_c \in V_c^{A_1 \ldots A_n} \otimes V^c_{A'_1 \ldots A'_n} \tag{2.20}$$

(note that this decomposition is basis independent), which may be used to relate the quantum trace and the standard trace of bras and kets via

$$\mathrm{Tr}X = \sum_c \frac{1}{d_c} \widetilde{\mathrm{Tr}} X_c, \qquad \widetilde{\mathrm{Tr}}X = \sum_c d_c \mathrm{Tr} X_c. \tag{2.21}$$

Note that these are the same when the overall charge of the system is the vacuum charge (or any Abelian charge for that matter).

We also need to define the *partial* traces for anyons. Since we have not yet introduced braiding, in order to take the partial trace over a single anyon B, the planar structure requires that it must be one of the two outer anyons (i.e. the first or last in the lineup). Physically, this corresponds to the fact that one cannot treat the subsystem excluding B as independent of B if this anyon is still located in the midst of the remaining anyons. The partial quantum trace over B of an operator $X \in V^{A_1,\ldots,A_n,B}_{A'_1,\ldots,A'_n,B'}$

is defined by looping only the line for anyon B back on itself

$\widetilde{\mathrm{Tr}}_B X =$ 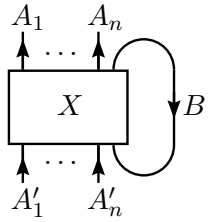

(2.22)

and for $X \in V^{B,A_1,\ldots,A_n}_{B',A'_1,\ldots,A'_n}$ as

$\widetilde{\mathrm{Tr}}_B X =$ 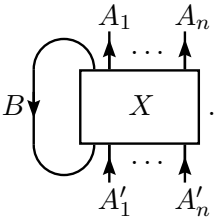

. (2.23)

To relate the partial quantum trace to the partial trace, we implement factors for the quantum dimensions of the overall charges of the operator before *and* after the partial trace

$$\mathrm{Tr}_B X = \sum_{c,f} \frac{d_f}{d_c} \left[\widetilde{\mathrm{Tr}}_B X_c\right]_f , \qquad \widetilde{\mathrm{Tr}}_B X = \sum_{c,f} \frac{d_c}{d_f} \left[\mathrm{Tr}_B X_c\right]_f , \tag{2.24}$$

where

$$\widetilde{\mathrm{Tr}}_B X_c = \sum_f \left[\widetilde{\mathrm{Tr}}_B X_c\right]_f , \qquad \left[\widetilde{\mathrm{Tr}}_B X_c\right]_f \in V_f^{A_1,\ldots,A_n} \otimes V^f_{A'_1,\ldots,A'_n} . \tag{2.25}$$

The partial trace and partial quantum trace over the subsystem of anyons $B = \{B_1, \ldots, B_n\}$ that are sequential outer lines (on either, possibly alternating, sides) of an operator is defined by iterating the partial quantum trace on the B anyons

$$\mathrm{Tr}_B = \mathrm{Tr}_{B_1} \ldots \mathrm{Tr}_{B_n} , \qquad \widetilde{\mathrm{Tr}}_B = \widetilde{\mathrm{Tr}}_{B_1} \ldots \widetilde{\mathrm{Tr}}_{B_n} \tag{2.26}$$

Iterating these over all the anyons of a system returns the trace and quantum trace, respectively, as they should.

Using Eq. (2.17) and the fact that tadpole diagrams evaluate to zero, we may calculate the partial quantum trace for basis elements of two-particle operators

$$\widetilde{\mathrm{Tr}}_B$$ 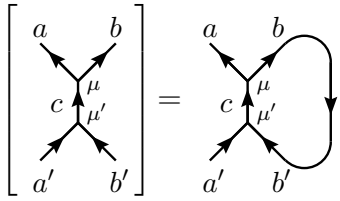 $$= \sum_{e,\alpha,\beta} \left[\left(F^{ab}_{a'b'}\right)^{-1}\right]_{(c,\mu,\mu')(e,\alpha,\beta)}$$ 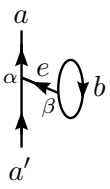

$$= \left[\left(F^{ab}_{ab}\right)^{-1}\right]_{(c,\mu,\mu')1}$$ 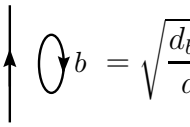 $$= \sqrt{\frac{d_b d_c}{d_a}}\delta_{\mu\mu'}$$ 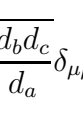 $$. \qquad (2.27)$$

From this, we see that the partial trace acting on ket-bra elements seems to behave as the usual partial trace, and one might think it should be treated as such. However, things are a bit more subtle than this, since these bras and kets do not have the usual tensor product structure. When considering tensor products of operators, it is the partial quantum trace that behaves in the appropriate manner for a partial traces (i.e. as in the usual basis independent definition of partial trace), indicating that this should be treated as the usual notion of partial trace. Specifically, tracing over the set of anyons B on which the operator Y acts, we have

$$\widetilde{\mathrm{Tr}}_B\left[X \otimes Y\right] = X\widetilde{\mathrm{Tr}}Y \qquad (2.28)$$

$$\mathrm{Tr}_B\left[X \otimes Y\right] = \sum_{a,b,c} N^c_{ab} X_a \mathrm{Tr} Y_b. \qquad (2.29)$$

2.5 Braiding

The unitary braiding operations of pairs of anyons, also called R-moves, are written as

$$R_{ab} =$$  $$, \qquad R^{\dagger}_{ab} = R^{-1}_{ab} =$$  $$, \qquad (2.30)$$

which are defined through their application to basis vectors:

$$R_{ab}\left|a,b;c,\mu\right\rangle = \sum_{\nu}\left[R^{ab}_{c}\right]_{\mu\nu}\left|b,a;c,\nu\right\rangle \qquad (2.31)$$

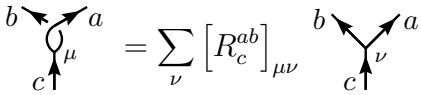

$$= \sum_{\nu}\left[R^{ab}_{c}\right]_{\mu\nu}$$ $$\qquad (2.32)$$

and similarly for R^{-1}, which, by unitarity, satisfy $\left[\left(R^{ab}_{c}\right)^{-1}\right]_{\mu\nu} = \left[R^{ba}_{c}\right]^{*}_{\nu\mu}$.

For braiding to be consistent with fusion, it must satisfy constraints (the Hexagon equations), which essentially impose the property that lines may be passed over or

under vertices respectively (i.e. braiding commutes with fusion), and which imply the usual Yang-Baxter relation for braids.

With the ability to braid, one also gains the ability to trace out any anyon in a system, not just those situated at one of the two outer positions of a planar diagram. To do so, one simply uses a series of braiding operations to move the anyon to one of the outside positions. In general, if one applies a different series of braids to move the anyon to the outside position before tracing, it will give a different outcome. Consequently, the braiding path applied to an anyon before closing its charge line should be included as part of the definition of the partial (quantum) trace. Physically, this corresponds to specifying the path (with respect to the other anyons) by which the traced anyon is removed from the system in consideration. In this paper, we will diagrammatically indicate the removal path of the anyon being traced out whenever the issue arises.

The braiding matrices satisfy the ribbon property

$$\sum_{\lambda} \left[R_c^{ab}\right]_{\mu\lambda} \left[R_c^{ba}\right]_{\lambda\nu} = \frac{\theta_c}{\theta_a \theta_b} \delta_{\mu\nu} \tag{2.33}$$

where θ_a is a root of unity called the topological spin of a, defined by

$$\theta_a = \theta_{\bar{a}} = d_a^{-1} \widetilde{\mathrm{Tr}} R_{aa} = \sum_{c,\mu} \frac{d_c}{d_a} \left[R_c^{aa}\right]_{\mu\mu} = \frac{1}{d_a}$$

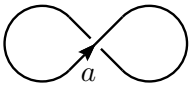

. (2.34)

When applicable, this is related to s_a, the (ordinary angular momentum) spin or CFT conformal scaling dimension of a, by

$$\theta_a = e^{i2\pi s_a}. \tag{2.35}$$

The topological S-matrix is defined by

$$S_{ab} = \mathcal{D}^{-1} \widetilde{\mathrm{Tr}} \left[R_{ba} R_{ab}\right] = \mathcal{D}^{-1} \sum_c N_{ab}^c \frac{\theta_c}{\theta_a \theta_b} d_c = \frac{1}{\mathcal{D}}$$

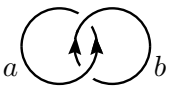

. (2.36)

One can see from this that $S_{ab} = S_{ba} = S_{\bar{a}b}^*$ and $d_a = S_{1a}/S_{11}$. A useful property for removing loops from lines is

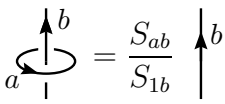

(2.37)

An anyon model is "modular" and corresponds to a TQFT (topological quantum field theory), if its monodromy is non-degenerate, i.e. for each $a \neq 1$, there is some b such that $R_{ba} R_{ab} \neq \mathbb{I}_{ab}$, which is the case iff the topological S-matrix is unitary. For such theories, the S-matrix, together with $T_{ab} = \theta_a \delta_{ab}$ represent the generators of the modular group PSL $(2, \mathbb{Z})$.

The monodromy scalar component

$$M_{ab} = \frac{\widetilde{\mathrm{Tr}}\left[R_{ba}R_{ab}\right]}{\widetilde{\mathrm{Tr}}\mathbb{I}_{ab}} = \frac{1}{d_a d_b}$$ 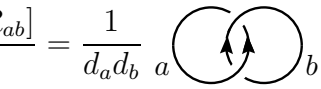 $$= \frac{S_{ab}S_{11}}{S_{1a}S_{1b}} \tag{2.38}$$

is an important quantity, typically arising in interference terms, such as those occurring in experiments that probe anyonic charge. It may also be written the $1,1$ component of the operator $B^2 = F^{-1}R^2F$. Since B^2 is a unitary operator, we must have $|M_{ab}| \leq 1$. Indeed unitarity implies that when $|M_{ab}| = 1$, only the $1,1$ element of B^2 is non-zero, hence

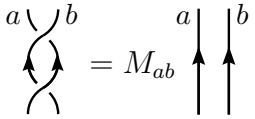 (2.39)

so that the braiding of a and b is Abelian. The monodromy of a and b is trivial if $M_{ab} = 1$. If $N_{ab}^c \neq 0$ and $|M_{be}| = 1$ for some e, then the relation

$$M_{ce} = M_{ae}M_{be} \tag{2.40}$$

follows from the diagrammatic equation

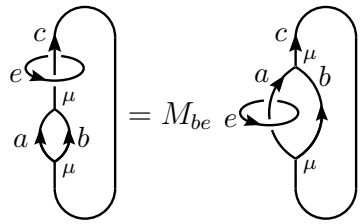 (2.41)

2.6 States and Density Matrices

To describe the state of anyons in a system using a state vector, one must specify all the splitting channels starting from vacuum. For example, in order to have anyons with charges a and b with overall charge c, one must also have a $\bar{c}$ charge somewhere, and one would write a general state of this form as

$$\begin{aligned} |\Psi\rangle &= \sum_{a,b,c,\mu} \psi_{a,b,c,\mu} \left|a,b;c,\mu\right\rangle \left|c,\bar{c};1\right\rangle \\ &= \sum_{a,b,c,\mu} \frac{\psi_{a,b,c,\mu}}{\left(d_a d_b d_c\right)^{1/4}}$$ 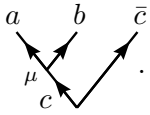 $$. \end{aligned} \tag{2.42}$$

Unfortunately, describing states in this manner can become cumbersome, and, as usual, does not naturally accommodate the restriction to subsystems, so it is better for us to use the density matrix formalism.

The density matrix for an arbitrary two anyon system is

$$\rho = \sum_{\substack{a,a',b,b' \\ c,\mu,\mu'}} \rho_{(a,b,c,\mu)(a',b',c,\mu')} \frac{1}{d_c} |a,b;c,\mu\rangle \langle a',b';c,\mu'|$$

$$= \sum_{\substack{a,a',b,b' \\ c,\mu,\mu'}} \frac{\rho_{(a,b,c,\mu)(a',b',c,\mu')}}{\left(d_a d_b d_{a'} d_{b'} d_c^2\right)^{1/4}}$$

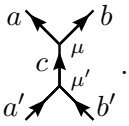

. (2.43)

The overall charge c must match up between the bra and the ket because of charge conservation. The normalization is chosen such that the trace condition for density matrices takes the form

$$\widetilde{\mathrm{Tr}}\,[\rho] = \sum_{a,b,c,\mu} \rho_{(a,b,c,\mu)(a,b,c,\mu)} = 1 \tag{2.44}$$

The factor $1/d_c$ could, of course, be absorbed into $\rho_{(a,b,c,\mu)(a',b',c,\mu')}$ (as a matter of convention), but then the d_c would appear in the summand of Eq. (2.44). Furthermore, the density matrix is written this way so that one can naturally think of it as $\rho = \widetilde{\mathrm{Tr}}_{\overline{C}}\,[\rho']$, the partial quantum trace over $\overline{C}$ of a density matrix that describes the actual entire system

$$\rho' = \sum_{\substack{a,b,c,\mu \\ a',b',c',\mu'}} \rho_{(a,b,c,\mu)(a',b',c',\mu')} |a,b;c,\mu\rangle |c,\bar{c};1\rangle \langle c',\overline{c'};1| \langle a',b';c',\mu'|$$

$$= \sum_{\substack{a,b,c,\mu \\ a',b',c',\mu'}} \frac{\rho_{(a,b,c,\mu)(a',b',c',\mu')}}{\left(d_a d_b d_c d_{a'} d_{b'} d_{c'}\right)^{1/4}}$$

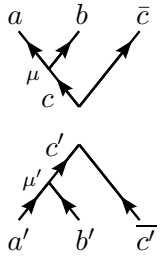

(2.45)

which only has vacuum overall charge. In other words, the entire system really has trivial total anyonic charge, but by restricting our attention to some subset of anyons, we have a reduced subsystem with overall charge c. Tracing over the $\overline{C}$ anyon (which imposes $c = c'$) physically represents the fact that it is no longer included in the system of interest, and cannot be brought back to interact with the A and B anyons. Because of this, we are restricted to a subsystem which may only have incoherent superpositions of different overall charges c (i.e. one must keep track of the $\overline{C}$ anyon to allow access to coherent superpositions). The manifestation of this property in ρ is exhibited by the charge c matching in the bra and the ket (or diagrammatically as the charge c line connecting μ and μ'). The generalization to density matrices of arbitrary numbers of anyons should be clear.

When considering the combination of two sets of anyons $A = \{A_1, \ldots, A_m\}$ and $B = \{B_1, \ldots, B_n\}$, the anyons of system A are unentangled with those of system B if the density matrix of the combined system is the tensor product (in some basis)

of density matrices of the two systems $\rho^{AB} = \rho^A \otimes \rho^B$. This essentially means the creation histories of the two different systems do not involve each other. There is a specific aspect of entanglement in anyonic systems that we will call *anyonic charge entanglement*, which is encoded in the anyonic charge lines connecting anyons. The systems of anyons A and B are said to have no anyonic charge entanglement between them if $\rho^{AB} \in V_{A'_1,\ldots,A'_m}^{A_1,\ldots,A_m} \otimes V_{B'_1,\ldots,B'_n}^{B_1,\ldots,B_n}$. This is represented diagrammatically as being able to write the combined state such that there are no non-trivial charge lines connecting the anyons of A with those of B.

3 Mach-Zehnder Interferometer

In this section, we consider, in detail, a Mach-Zehnder type interferometer [80,81] (see Fig. 1) for quasiparticles with non-Abelian anyonic braiding statistics, extending the analysis begun in Ref. [82]. This will serve as a prototypic model of interferometry experiments with anyons, and the methods used in its analysis readily apply to other classes of interferometers (e.g. the FQH double point-contact interferometer considered in Section 4). This interferometer was first considered for non-Abelian anyons in Ref. [83], but only for anyon models described by a discrete gauge theory-type formalism in which individual particles are assumed to have internal Hilbert spaces, and which use probe anyons that are all identical and have trivial self-braiding. Unfortunately, this excludes perhaps the most important class of anyon models – those describing the fractional quantum Hall states – so we must dispense with such restrictions. We will abstract to an idealized system that supports an arbitrary anyon model and also allows for a number of desired manipulations to be effected. Specifically, without concern for ways to physically actualize such manipulations, we posit the experimental abilities to: (1) produce, isolate, and position desired anyons, (2) provide anyons with some manner of propulsion to produce a beam of probe anyons, (3) construct lossless beam-splitters and mirrors, and (4) detect the presence of a probe anyon at the output legs of the interferometer.

The target anyon A is the composite of all anyons $A_1, A_2, \ldots$ that are located inside the central interferometry region, and so may be in a superposition of states with different total anyonic charges. Since these anyons are treated collectively by the experiment, we ignore their individuality and consider them as a single anyon A capable of charge superposition. We will similarly allow the probe anyons, $B_1, \ldots, B_N$ to be treated as capable of charge superposition (though this would certainly be more difficult to physically realize). The probe anyons are sent as a beam into the interferometer through two possible input channels. They pass through a beam splitter T_1, are reflected by mirrors around the central target region, pass through a second beam splitter T_2, and then are detected at one of the two possible output channels by the detectors D_s. When a probe anyon B passes through the bottom path of the interferometer, the state acquires the phase $e^{i\theta_1}$, which results

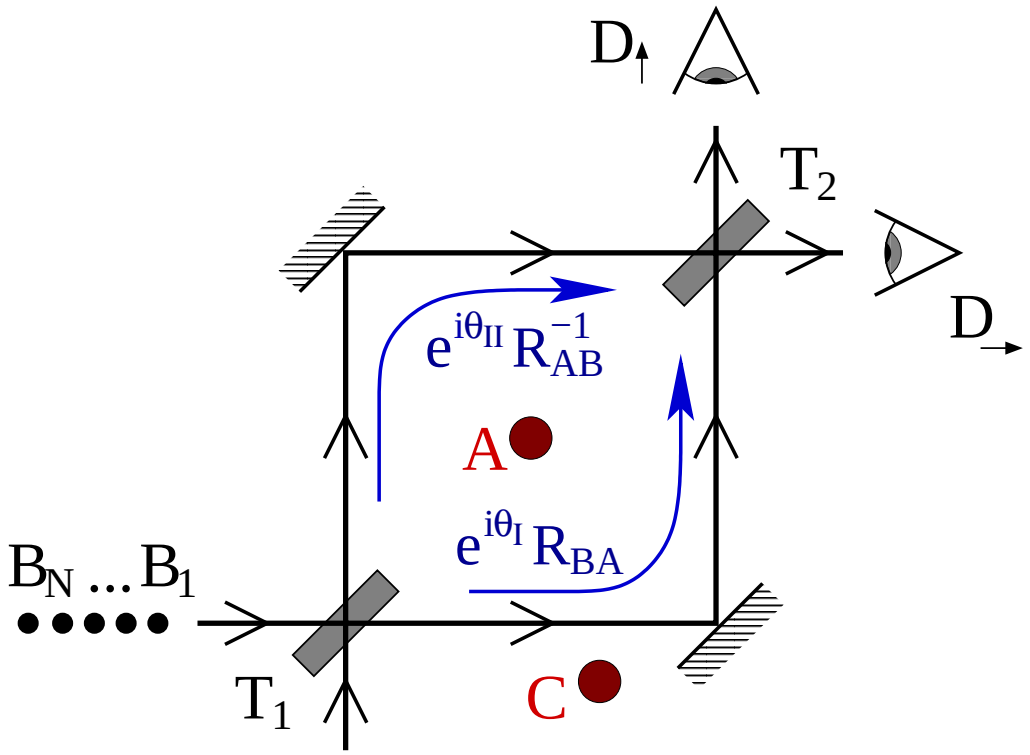

Fig. 1. A Mach-Zehnder interferometer for an anyonic system. The target anyon(s) A in the central region shares entanglement only with the anyon(s) C outside this region. A beam of probe anyons $B_1, \ldots, B_N$ is sent through the interferometer, where T_j are beam splitters, and detected at one of the two possible outputs by D_s.

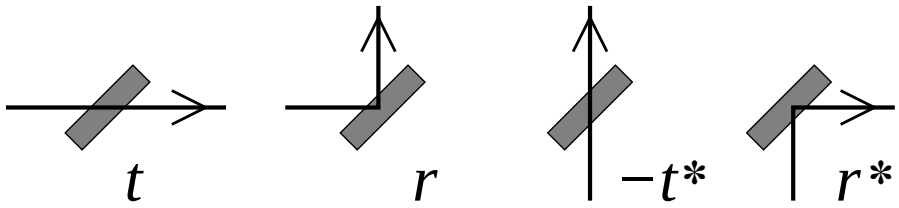

Fig. 2. The transmission and reflection coefficients for a beam splitter.

from background Aharonov-Bohm interactions [76], path length differences, phase shifters, etc., and is also acted upon by the braiding operator R_{BA}, which is strictly due to the braiding statistics between the probe and target anyons. Similarly, when the probe passes through the top path of the interferometer, the state acquires the phase $e^{i\theta_{\rm II}}$ and is acted on by R^{-1}_{AB}.

Using the two-component vector notation

$$\begin{pmatrix} 1 \\ 0 \end{pmatrix} = |{\rightarrow}\rangle\,, \quad \begin{pmatrix} 0 \\ 1 \end{pmatrix} = |{\uparrow}\rangle \tag{3.1}$$

to indicate the direction (horizontal or vertical) a probe anyon is traveling through

the interferometer at any point, the lossless beam splitters [84] (see Fig. 2) are represented by

$$T_j = \begin{bmatrix} t_j & r_j^* \\ r_j & -t_j^* \end{bmatrix} \tag{3.2}$$

(for $j = 1, 2$), where $|t_j|^2 + |r_j|^2 = 1$. We note that these matrices could be multiplied by overall phases without affecting any of the results, since such phases are not distinguished by the two paths.

When considering operations involving non-Abelian anyons, it is important to keep track of all other anyons with which there is non-trivial entanglement. Indeed, if these additional particles are not tracked or are physically inaccessible, one should trace them out of the system, forgoing the ability to use them to form coherent superpositions of anyonic charge. We assume that the target anyon has no initial entanglement with the probe anyons, so their systems will be combined as tensor products, with no non-trivial charge lines connecting them before they interact in the interferometer.

The target system involves the target anyon A and the anyon C which is the only one entangled with A that is kept physically accessible. Recall that these anyons may really represent multiple quasiparticles that are being treated collectively, but as long as we are not interested in operations involving the individual quasiparticles, they can be treated as a single anyon. The density matrix of the target system is

$$\begin{aligned} \rho^A &= \sum_{a,a',c,c',f,\mu,\mu'} \rho^A_{(a,c;f,\mu)(a',c';f,\mu')} \frac{1}{d_f} |a,c;f,\mu\rangle \langle a',c';f,\mu'| \\ &= \sum_{a,a',c,c',f,\mu,\mu'} \frac{\rho^A_{(a,c;f,\mu)(a',c';f,\mu')}}{\left(d_a d_{a'} d_c d_{c'} d_f^2\right)^{1/4}} \end{aligned} \tag{3.3}$$

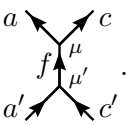

We will assume that the probe anyons are also not entangled with each other, and that they are all identical (or, more accurately, belong to an ensemble of particles all described by the density matrix ρ^B). We will consider generalizations of the probe anyons in Section 3.5. Such generalizations complicate the bookkeeping of the calculation, but will have qualitatively similar results. A probe system involves the probe anyon B, which is sent through the interferometer entering the horizontal leg $s = \rightarrow$, and the anyon D which is entangled with B and will be sent off to the (left) side. We will write the directional index s of the probe particle as a subscript on its anyonic charge label, i.e. b_s. The density matrix of a probe system is

$$\rho^B = \sum_{b,b',d,d',h,\lambda,\lambda'} \rho^B_{(d,b_\rightarrow;h,\lambda)(d',b'_\rightarrow;h,\lambda')} \frac{1}{d_h} |d, b_\rightarrow; h, \lambda\rangle \langle d', b'_\rightarrow; h, \lambda'|$$

$$= \sum_{b,b',d,d',h,\lambda,\lambda'} \frac{\rho^B_{(d,b_\rightarrow;h,\lambda)(d',b'_\rightarrow;h,\lambda')}}{\left(d_d d_{d'} d_b d_{b'} d_h^2\right)^{1/4}}$$

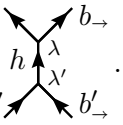

. (3.4)

The unitary operator representing a probe anyon passing through the interferometer is given by

$$U = T_2 \Sigma T_1 \tag{3.5}$$

$$\Sigma = \begin{bmatrix} 0 & e^{i\theta_{\mathrm{II}}} R_{AB}^{-1} \\ e^{i\theta_{\mathrm{I}}} R_{BA} & 0 \end{bmatrix}. \tag{3.6}$$

This can be written diagrammatically as

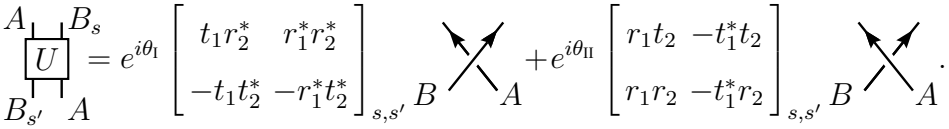

. (3.7)

The position of the anyon C with respect to the other anyons must be specified, and we will take it to be located below the central interferometry region and slightly to the right of A. (The specification "slightly to the right" merely indicates how the diagrams are to be drawn, and has no physical consequence.) For this choice of positioning, the operator

$$V = \begin{bmatrix} R_{CB}^{-1} & 0 \\ 0 & R_{CB}^{-1} \end{bmatrix} =$$

(3.8)

represents the braiding of C with the probe. In Section 3.4, we will give the results for situating the anyon(s) C in different locations outside the central interferometry region, and find that the qualitative behavior is essentially the same.

After a probe anyon B is measured at one of the detectors, it no longer interests us, and we remove it along with its entangled partner D from the vicinity of the target anyon system. Mathematically, this means we take the tensor product of the probe and target systems, evolve them with VU (which sends the probe through the interferometer) to get

$$\rho = VU \left(\rho^B \otimes \rho^A\right) U^\dagger V^\dagger, \tag{3.9}$$

apply the usual orthogonal measurement collapse projection

$$\Pr(s) = \widetilde{\mathrm{Tr}}\left[\rho \Pi_s\right] \tag{3.10}$$

$$\rho \mapsto \frac{1}{\Pr(s)} \Pi_s \rho \Pi_s \tag{3.11}$$

with $\Pi_s = |s\rangle\langle s|$ for the outcome s, and then finally trace out the anyons B and D. Since the probe anyons are all initially unentangled, we may obtain their effect on the target system by considering that of each probe individually.

3.1 One Probe

We begin by considering the effect of a single probe with definite anyonic charge b, i.e. $\rho^b = \left|\bar{b}, b_{\rightarrow}; 1\right\rangle\left\langle\bar{b}, b_{\rightarrow}; 1\right|$, and return to general ρ^B immediately afterwards. For a particular component of the target anyons' density matrix, the relevant diagram that must be evaluated for a single probe measurement is

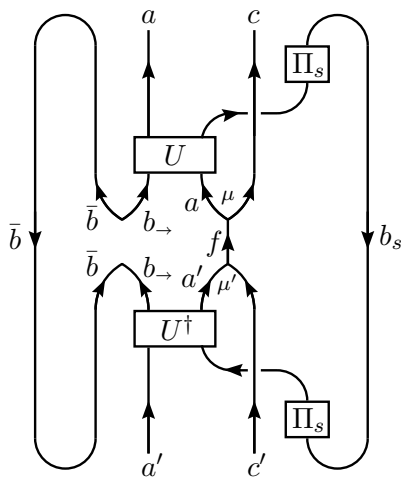

(3.12)

For the outcome $s = \rightarrow$, this is

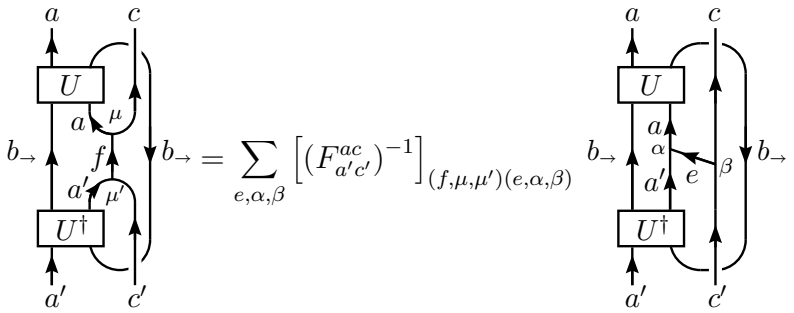

$$= \sum_{e,\alpha,\beta} \left[(F^{ac}_{a'c'})^{-1} \right]_{(f,\mu,\mu')(e,\alpha,\beta)}$$

$$\times \Bigg\{ |t_1|^2 \, |r_2|^2$$

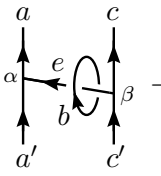

$$+ t_1 r_1^* r_2^* t_2^* e^{i(\theta_{\rm I}-\theta_{\rm II})}$$

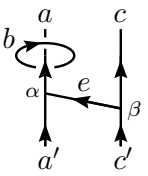

$$+ t_1^* r_1 t_2 r_2 e^{-i(\theta_{\rm I}-\theta_{\rm II})}$$

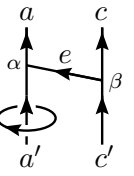

$$+ |r_1|^2 \, |t_2|^2$$

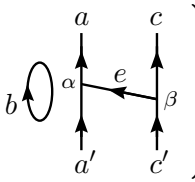

$$\Bigg\}$$

$$= d_b \sum_{e,\alpha,\beta} \left[(F^{ac}_{a'c'})^{-1} \right]_{(f,\mu,\mu')(e,\alpha,\beta)} \vec{p}_{aa'e,b}$$

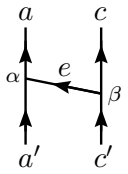

$$= d_b \sum_{\substack{e,\alpha,\beta \\ f',\nu,\nu'}} \left[(F^{ac}_{a'c'})^{-1} \right]_{(f,\mu,\mu')(e,\alpha,\beta)} \left[F^{ac}_{a'c'} \right]_{(e,\alpha,\beta)(f',\nu,\nu')} \vec{p}_{aa'e,b}$$

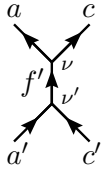

(3.13)

where we have defined

$$\begin{aligned} \vec{p}_{aa'e,b} = & \, |t_1|^2 \, |r_2|^2 \, M_{eb} + t_1 r_1^* r_2^* t_2^* e^{i(\theta_{\rm I}-\theta_{\rm II})} M_{ab} \\ & + t_1^* r_1 t_2 r_2 e^{-i(\theta_{\rm I}-\theta_{\rm II})} M^*_{a'b} + |r_1|^2 \, |t_2|^2 \end{aligned} \tag{3.14}$$

and have used Eqs. (2.37,2.38) to remove the b loops. A similar calculation for the $s = \uparrow$ outcome gives

$$\begin{aligned} p^{\uparrow}_{aa'e,b} = & \, |t_1|^2 \, |t_2|^2 \, M_{eb} - t_1 r_1^* r_2^* t_2^* e^{i(\theta_{\rm I}-\theta_{\rm II})} M_{ab} \\ & - t_1^* r_1 t_2 r_2 e^{-i(\theta_{\rm I}-\theta_{\rm II})} M^*_{a'b} + |r_1|^2 \, |r_2|^2 \, . \end{aligned} \tag{3.15}$$

From this, inserting the appropriate coefficients and normalization factors, we find the reduced density matrix of the target anyons after a single probe measurement

with outcome s:

$$\begin{aligned}
\rho^A(s) &= \frac{1}{\Pr(s)}\widetilde{\mathrm{Tr}}_{\overline{B},B}\left[\Pi_s\rho\Pi_s\right] \\
&= \sum_{\substack{a,a',c,c',f,\mu,\mu' \\ e,\alpha,\beta,f',\nu,\nu'}} \frac{\rho^A_{(a,c;f,\mu)(a',c';f,\mu')}}{\left(d_a d_{a'} d_c d_{c'} d_f^2\right)^{1/4}} \frac{p^s_{aa'e,b}}{\Pr(s)} \\
&\quad \times \left[\left(F^{ac}_{a'c'}\right)^{-1}\right]_{(f,\mu,\mu')(e,\alpha,\beta)} \left[F^{ac}_{a'c'}\right]_{(e,\alpha,\beta)(f',\nu,\nu')} \\
&= \sum_{\substack{a,a',c,c',f,\mu,\mu' \\ e,\alpha,\beta,f',\nu,\nu'}} \frac{\rho^A_{(a,c;f,\mu)(a',c';f,\mu')}}{\left(d_f d_{f'}\right)^{1/2}} \frac{p^s_{aa'e,b}}{\Pr(s)} \left[\left(F^{ac}_{a'c'}\right)^{-1}\right]_{(f,\mu,\mu')(e,\alpha,\beta)} \\
&\quad \times \left[F^{ac}_{a'c'}\right]_{(e,\alpha,\beta)(f',\nu,\nu')} |a,c;f',\nu\rangle\langle a',c';f',\nu'| \qquad (3.16)
\end{aligned}$$

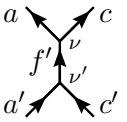

where the probability of measurement outcome s is found by additionally taking the quantum trace of the target system, which projects onto the $e = 1$ components, giving

$$\Pr(s) = \widetilde{\mathrm{Tr}}\left[\rho\Pi_s\right] = \sum_{a,c,f,\mu} \rho^A_{(a,c;f,\mu)(a,c;f,\mu)} p^s_{aa1,b}. \qquad (3.17)$$

We note that

$$p^{\rightarrow}_{aa1,b} = |t_1|^2 |r_2|^2 + |r_1|^2 |t_2|^2 + 2\mathrm{Re}\left\{t_1 r_1^* r_2^* t_2^* e^{i(\theta_{\mathrm{I}}-\theta_{\mathrm{II}})} M_{ab}\right\} \qquad (3.18)$$

$$p^{\uparrow}_{aa1,b} = |t_1|^2 |t_2|^2 + |r_1|^2 |r_2|^2 - 2\mathrm{Re}\left\{t_1 r_1^* r_2^* t_2^* e^{i(\theta_{\mathrm{I}}-\theta_{\mathrm{II}})} M_{ab}\right\} \qquad (3.19)$$

give a well-defined probability distribution in s (i.e. $0 \leq p^s_{aa1,b} \leq 1$ and $p^{\rightarrow}_{aa1,b} + p^{\uparrow}_{aa1,b} = 1$).

The quantity

$$t_1 r_1^* t_2^* r_2^* e^{i(\theta_{\mathrm{I}}-\theta_{\mathrm{II}})} \equiv T e^{i\theta} \qquad (3.20)$$

determines the visibility of quantum interference in this experiment, where varying θ allows one to observe the interference term modulation. The amplitude $T = |t_1 r_1 t_2 r_2|$ is maximized by $|t_j| = |r_j| = 1/\sqrt{2}$. In realistic experiments, the experimental parameters t_j, r_j, θ_{I}, and θ_{II} will have some variance, even for a single probe, that gives rise to some degree of phase incoherence. Averaging over some distribution in θ, one finds that $e^{i\theta}$ in the interference terms should effectively be replaced by $\left\langle e^{i\theta}\right\rangle = Q e^{i\theta_*}$. In this expression, $e^{i\theta_*}$ is the resulting effective phase, and $Q \in [0,1]$ is a suppression factor that reflects the interferometer's lack of coherence, and reduces the visibility of quantum interference. For the rest of the paper, we will ignore this issue and assume $Q = 1$, but it should always be kept in mind that success of any interferometry experiment is crucially dependent on Q being made as large as possible.

We can now obtain the result for general ρ^B by simply replacing $p^s_{aa'e,b}$ everywhere with

$$p^s_{aa'e,B} = \sum_b \Pr_B(b)\, p^s_{aa'e,b} \tag{3.21}$$

$$\Pr_B(b) = \sum_{d,h,\lambda} \rho^B_{(d,b_\rightarrow;h,\lambda)(d,b_\rightarrow;h,\lambda)}. \tag{3.22}$$

We will also use the notation $M_{aB} = \sum_b \Pr_B(b)\, M_{ab}$. That this replacement gives the appropriate results follows from the fact that we trace out the D anyon, and may be seen from

$$\widetilde{\mathrm{Tr}}_D\left[\rho^B\right] = \sum_{b,b',d,h,\lambda,\lambda'} \frac{\rho^B_{(d,b_\rightarrow;h,\lambda)(d,b'_\rightarrow;h,\lambda')}}{\left(d_d^2 d_b d_{b'} d_h^2\right)^{1/4}}$$

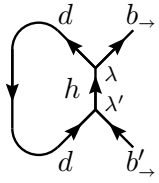

$$= \sum_{b,d,h,\lambda} \rho^B_{(d,b_\rightarrow;h,\lambda)(d,b_\rightarrow;h,\lambda)} \frac{1}{d_b}$$

$$= \sum_{b,d,h,\lambda} \rho^B_{(d,b_\rightarrow;h,\lambda)(d,b_\rightarrow;h,\lambda)} \frac{1}{d_b}$$

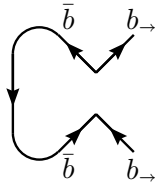

$$= \sum_b \Pr_B(b)\, \widetilde{\mathrm{Tr}}_{\bar{b}} \left|\bar{b}, b_\rightarrow; 1\right\rangle \left\langle \bar{b}, b_\rightarrow; 1\right|$$

$$= \widetilde{\mathrm{Tr}}_{\overline{B}} \sum_b \Pr_B(b) \left|\bar{b}, b_\rightarrow; 1\right\rangle \left\langle \bar{b}, b_\rightarrow; 1\right| \tag{3.23}$$

where we used Eq. (2.27) in the first step.

3.2 N Probes

The result for N initially unentangled identical probe particles sent through the interferometer may now be easily produced by iterating the single probe calculation. The string of measurement outcomes $(s_1, \ldots, s_N)$ occurs with probability

$$\Pr(s_1, \ldots, s_N) = \sum_{a,c,f,\mu} \rho^A_{(a,c;f,\mu)(a,c;f,\mu)} p^{s_1}_{aa1,B} \cdots p^{s_N}_{aa1,B} \tag{3.24}$$

and results in the measured target anyon reduced density matrix

$$\rho^A(s_1,\ldots,s_N) = \sum_{\substack{a,a',c,c',f,\mu,\mu' \\ e,\alpha,\beta,f',\nu,\nu'}} \frac{\rho^A_{(a,c;f,\mu)(a',c';f,\mu')}}{(d_f d_{f'})^{1/2}} \frac{p_{aa'e,B}^{s_1}\cdots p_{aa'e,B}^{s_N}}{\Pr(s_1,\ldots,s_N)}$$
$$\times \left[(F^{ac}_{a'c'})^{-1}\right]_{(f,\mu,\mu')(e,\alpha,\beta)} [F^{ac}_{a'c'}]_{(e,\alpha,\beta)(f',\nu,\nu')} |a,c;f',\nu\rangle\langle a',c';f',\nu'| . \quad (3.25)$$

It is apparent that the specific order of the measurement outcomes is not important in the result, but that only the total number of outcomes of each type matters, hence leading to a binomial distribution. We denote the total number of $s_j = \rightarrow$ in the string of measurement outcomes as n, and cluster together all results with the same n. Defining (for arbitrary p and q)

$$W_N(n;p,q) = \frac{N!}{n!\,(N-n)!} p^n q^{N-n} \quad (3.26)$$

the probability of measuring n of the N probes at the horizontal detector is

$$\Pr_N(n) = \sum_{a,c,f,\mu} \rho^A_{(a,c;f,\mu)(a,c;f,\mu)} W_N\left(n; p^{\rightarrow}_{aa1,B}, p^{\uparrow}_{aa1,B}\right) \quad (3.27)$$

and these measurements produce the target anyon reduced density matrix

$$\rho^A_N(n) = \sum_{\substack{a,a',c,c',f,\mu,\mu' \\ e,\alpha,\beta,f',\nu,\nu'}} \frac{\rho^A_{(a,c;f,\mu)(a',c';f,\mu')}}{(d_f d_{f'})^{1/2}} \frac{W_N\left(n; p^{\rightarrow}_{aa'e,B}, p^{\uparrow}_{aa'e,B}\right)}{\Pr_N(n)}$$
$$\times \left[(F^{ac}_{a'c'})^{-1}\right]_{(f,\mu,\mu')(e,\alpha,\beta)} [F^{ac}_{a'c'}]_{(e,\alpha,\beta)(f',\nu,\nu')} |a,c;f',\nu\rangle\langle a',c';f',\nu'| . \quad (3.28)$$

In Ref. [82], we obtained the reduced density matrix that ignores the measurement outcomes and describes the decoherence (rather than the precise details of collapse) due to the probe measurements. We find this density matrix by averaging over n, giving us the result in Eq. (15c) of [82], though for more general target and probe systems

$$\rho^A_N = \sum_{n=0}^{N} \Pr_N(n)\,\rho^A_N(n)$$
$$= \sum_{\substack{a,a',c,c',f,\mu,\mu' \\ e,\alpha,\beta,f',\nu,\nu'}} \frac{\rho^A_{(a,c;f,\mu)(a',c';f,\mu')}}{(d_f d_{f'})^{1/2}} \left(|t_1|^2 M_{eB} + |r_1|^2\right)^N$$
$$\times \left[(F^{ac}_{a'c'})^{-1}\right]_{(f,\mu,\mu')(e,\alpha,\beta)} [F^{ac}_{a'c'}]_{(e,\alpha,\beta)(f',\nu,\nu')} |a,c;f',\nu\rangle\langle a',c';f',\nu'| \quad (3.29)$$

where we used

$$\sum_{n=0}^{N} W_N\left(n; p^{\rightarrow}_{aa'e,B}, p^{\uparrow}_{aa'e,B}\right) = \left(p^{\rightarrow}_{aa'e,B} + p^{\uparrow}_{aa'e,B}\right)^N$$
$$= \left(|t_1|^2 M_{eB} + |r_1|^2\right)^N . \tag{3.30}$$

The interferometry experiment distinguishes anyonic charges in the target by their values of $p^s_{aa1,B}$, which determine the possible measurement distributions. Different anyonic charges with the same probability distributions of probe outcomes are indistinguishable by such probes, and so should be grouped together into distinguishable subsets. We define $\mathcal{C}_\kappa$ for $\kappa = 1, \ldots, m \leq |\mathcal{C}|$ to be the maximal disjoint subsets of $\mathcal{C}$ such that $p^{\rightarrow}_{aa1,B} = p_\kappa$ for all $a \in \mathcal{C}_\kappa$, i.e.

$$\mathcal{C}_\kappa \equiv \left\{a \in \mathcal{C} : p^{\rightarrow}_{aa1,B} = p_\kappa\right\}. \tag{3.31}$$

Note that $p^{\rightarrow}_{aa1,B} = p^{\rightarrow}_{a'a'1,B}$ (for two different charges a and a') iff

$$\mathrm{Re}\left\{t_1 r_1^* r_2^* t_2^* e^{i(\theta_{\mathrm{I}} - \theta_{\mathrm{II}})} M_{aB}\right\} = \mathrm{Re}\left\{t_1 r_1^* r_2^* t_2^* e^{i(\theta_{\mathrm{I}} - \theta_{\mathrm{II}})} M_{a'B}\right\} \tag{3.32}$$

which occurs either when:

(i) at least one of t_1, t_2, r_1, or r_2 is zero, or

(ii) $|M_{aB}| \cos(\theta + \varphi_a) = |M_{a'B}| \cos(\theta + \varphi_{a'})$, where $\theta = \arg\left(t_1 r_1^* r_2^* t_2^* e^{i(\theta_{\mathrm{I}} - \theta_{\mathrm{II}})}\right)$ and $\varphi_a = \arg(M_{aB})$.

If condition (i) is satisfied, then there is no interference and $\mathcal{C}_1 = \mathcal{C}$ (all target anyonic charges give the same probe measurement distribution). Condition (ii) is generically [2] only satisfied when $M_{aB} = M_{a'B}$, but may be non-generically satisfied by setting $\theta = -\arg\{M_{aB} - M_{a'B}\} \pm \frac{\pi}{2}$. With this notation, we may write

$$\Pr_N(n) = \sum_\kappa \Pr_A(\kappa)\, W_N(n; p_\kappa, 1 - p_\kappa) \tag{3.33}$$

$$\Pr_A(\kappa) = \sum_{a \in \mathcal{C}_\kappa, c, f, \mu} \rho^A_{(a,c;f,\mu)(a,c;f,\mu)}. \tag{3.34}$$

We emphasize that if the parameters t_j, r_j and θ in the experiment are known and adjustable, then the measurements may be used to gather information regarding the quantities M_{ab}, which, through its relation to the topological S-matrix, may be used to properly identify the anyon model that describes an unknown system [85].

In Sections 3.2.1 and 3.2.2, we will show that, as $N \to \infty$, the fraction $r = n/N$ of measurement outcomes will be found to go to $r = p_\kappa$ with probability $\Pr_A(\kappa)$, and

[2] The term "generic" is used in this paper only in reference to the collection of interferometer parameters t_j, r_j, θ_{I}, and θ_{II}.

the target anyon density matrix will generically collapse onto the corresponding "fixed states" given by

$$\rho_{\kappa}^{A} = \sum_{\substack{a,a',c,c',f,\mu,\mu' \\ e,\alpha,\beta,f',\nu,\nu'}} \frac{\rho^{A}_{(a,c;f,\mu)(a',c';f,\mu')}}{\left(d_f d_{f'}\right)^{1/2}} \Delta_{aa'e,B}\left(p_\kappa\right) \times \left[\left(F^{ac}_{a'c'}\right)^{-1}\right]_{(f,\mu,\mu')(e,\alpha,\beta)} \left[F^{ac}_{a'c'}\right]_{(e,\alpha,\beta)(f',\nu,\nu')} |a,c;f',\nu\rangle \langle a',c';f',\nu'| \tag{3.35}$$

where

$$\Delta_{aa'e,B}\left(p_\kappa\right) = \begin{cases} \frac{1}{\Pr_A(\kappa)} \text{ if } p^{\rightarrow}_{aa'e,B} = 1 - p^{\uparrow}_{aa'e,B} = p_\kappa \text{ and } a,a' \in \mathcal{C}_\kappa \\ 0 \qquad\qquad\qquad\qquad \text{otherwise} \end{cases} . \tag{3.36}$$

Fixed state density matrices are left unchanged by probe measurements. We also emphasize that the condition: $p^{\rightarrow}_{aa'e,B} = 1 - p^{\uparrow}_{aa'e,B} = p_\kappa$ is equivalent to $M_{eB} = 1$ (noting that $M_{eB} = 1$ implies $M_{aB} = M_{a'B}$ and $a, a' \in \mathcal{C}_\kappa$). This gives the interpretation that the probes have the effect of collapsing superpositions of anyonic charges a and a' in the target that they can distinguish by monodromy ($M_{aB} \neq M_{a'B}$), *and* decohering all anyonic charge entanglement between the target anyon A and the anyons C outside the central interferometry region that the probes can "see" by monodromy, i.e. removing the components of the density matrix corresponding to e-channels with $M_{eB} \neq 1$. Non-generically, it is also possible to collapse onto "rogue states," for which the diagonal density matrix elements are all fixed and some of the off-diagonal elements have fixed magnitude, but phases that change depending on the measurement outcome (i.e. are "quasi-fixed"). Because rogue states occur only for specific, exactly precise experimental parameters, they will not actually survive measurement in realistic experiments. We note that if $M_{eB} = 1$ only for $e = 1$, then the probe distinguishes all charges, and the fixed states are given by

$$\rho^{A}_{\kappa_a} = \sum_{c} \frac{\Pr_A(c|a)}{d_a d_c} \mathbb{I}_{ac} = \sum_{c,f',\nu} \frac{\Pr_A(c|a)}{d_a d_c} |a,c;f',\nu\rangle \langle a,c;f',\nu| \tag{3.37}$$

where

$$\Pr_A(c|a) = \frac{\sum_{f,\mu} \rho^{A}_{(a,c;f,\mu)(a,c;f,\mu)}}{\sum_{c,f,\mu} \rho^{A}_{(a,c;f,\mu)(a,c;f,\mu)}}, \tag{3.38}$$

for which the target anyon A has definite charge and no entanglement with C. We give examples of fixed state density matrices for several significant anyon models in Section 3.6.

In principle, one may also consider the "many-to-many" experiment described in Ref. [83], where the target anyon system is replaced with a fresh one (described by the same initial density matrix) after each probe measurement. For this type

of experiment, the result for each probe is described by the single probe outcome probability, Eq. (3.17):

$$\Pr(s) = \sum_{a,c,f,\mu} \rho^{A}_{(a,c;f,\mu)(a,c;f,\mu)} p^{s}_{aa1,B}. \tag{3.39}$$

Thus, for N such probe measurements, the number n of $s =\!\rightarrow$ measurement outcomes will have the binomial distribution: $W_N(n; \Pr(\rightarrow), \Pr(\uparrow))$.

3.2.1 Large N

We would like to analyze the large N behavior of the measurements. This is essentially determined by $W_N(n; p_\kappa, 1-p_\kappa)$ and $\frac{W_N\left(n; p^{\rightarrow}_{aa'e,B}, p^{\uparrow}_{aa'e,B}\right)}{\Pr_N(n)}$, so we now consider these in detail. Of course, $W_N(n; p_\kappa, 1-p_\kappa)$ is just a familiar binomial distribution. Changing variables to the fraction $r = n/N$ of total probe measurement outcomes in the horizontal detector, the distribution in r is given by

$$w_N(r; p_\kappa, 1-p_\kappa) = W_N(rN; p_\kappa, 1-p_\kappa) N \tag{3.40}$$

and has mean and standard deviation

$$\overline{r} = p_\kappa \tag{3.41}$$

$$\Delta r = \sigma_\kappa \equiv \sqrt{p_\kappa (1-p_\kappa)/N}. \tag{3.42}$$

Taking N large and using Stirling's formula, this may be approximated by a Gaussian distribution

$$w_N(r; p_\kappa, 1-p_\kappa) \simeq \frac{1}{\sqrt{2\pi\sigma^2_\kappa}} e^{-\frac{(r-p_\kappa)^2}{2\sigma^2_\kappa}}. \tag{3.43}$$

Taking the limit $N \to \infty$ gives

$$\lim_{N\to\infty} w_N(r; p_\kappa, 1-p_\kappa) = \delta(r - p_\kappa) \tag{3.44}$$

(defined such that $\int_0^1 \delta(r-p)\, dr = 1$, when $p = 0$ or 1), so the resulting probability distribution for the measurement outcomes is

$$\Pr(r) = \lim_{N\to\infty} \Pr_N(r) = \sum_\kappa \Pr_A(\kappa)\, \delta(r - p_\kappa) \tag{3.45}$$

Thus, as $N \to \infty$, we will find the fraction of measurement outcomes $r \to p_\kappa$ with probability $\Pr_A(\kappa)$.

Though the probability of obtaining the outcome r which is away from the closest

p_κ vanishes as

$$w_N\left(r; p_\kappa, 1-p_\kappa\right) \sim \sqrt{N}\left(\frac{p_\kappa^r\left(1-p_\kappa\right)^{1-r}}{r^r\left(1-r\right)^{1-r}}\right)^N \tag{3.46}$$

for large N, the resulting density matrix should still be well defined for all r (at least for large, but finite N). In particular, we will use the positivity property of density matrices, in the form of the Cauchy-Schwarz type inequality $\rho_{\mu\mu}\rho_{\nu\nu} \geq \left|\rho_{\mu\nu}\right|^2$, to evince their large N behavior in terms of conditions on $p^s_{aa'e,B}$. From the quantity

$$\begin{aligned}\Delta_{N;aa'e,B}\left(r\right) &\equiv \frac{W_N\left(rN; p^{\rightarrow}_{aa'e,B}, p^{\uparrow}_{aa'e,B}\right)}{\Pr_N\left(rN\right)} \\ &= \left\{\sum_{\kappa'}\Pr_A\left(\kappa'\right)\left[\left(\frac{p_{\kappa'}}{p^{\rightarrow}_{aa'e,B}}\right)^r\left(\frac{1-p_{\kappa'}}{p^{\uparrow}_{aa'e,B}}\right)^{1-r}\right]^N\right\}^{-1}\end{aligned} \tag{3.47}$$

we can see that as $N \to \infty$, the $e = 1$ terms (those that determine the "diagonal" elements) behave as:

(i) $\Delta_{N;aa1,B}\left(r\right) \to \frac{1}{\Pr_A(\kappa_1)}$ for $a \in \mathcal{C}_{\kappa_1}$, if $\Pr_A\left(\kappa_1\right) \neq 0$ and $p^r_{\kappa_1}\left(1-p_{\kappa_1}\right)^{1-r} > p^r_\kappa\left(1-p_\kappa\right)^{1-r}$ for all $\kappa \neq \kappa_1$,

(ii) $\Delta_{N;aa1,B}\left(r\right) \to \frac{1}{\Pr_A(\kappa_1)+\Pr_A(\kappa_2)}$ for $a \in \mathcal{C}_{\kappa_1} \cup \mathcal{C}_{\kappa_2}$, if $\Pr_A\left(\kappa_1\right) + \Pr_A\left(\kappa_2\right) \neq 0$ and $p^r_{\kappa_1}\left(1-p_{\kappa_1}\right)^{1-r} = p^r_{\kappa_2}\left(1-p_{\kappa_2}\right)^{1-r} > p^r_\kappa\left(1-p_\kappa\right)^{1-r}$ for all $\kappa \neq \kappa_1, \kappa_2$, or

(iii) $\Delta_{N;aa1,B}\left(r\right) \to 0$ for $a \in \mathcal{C}_{\kappa_1}$, if there is some κ with $\Pr_A\left(\kappa\right) \neq 0$ and $p^r_\kappa\left(1-p_\kappa\right)^{1-r} > p^r_{\kappa_1}\left(1-p_{\kappa_1}\right)^{1-r}$.

If $a \in \mathcal{C}_{\kappa_1}$, where $p^r_{\kappa_1}\left(1-p_{\kappa_1}\right)^{1-r} > p^r_\kappa\left(1-p_\kappa\right)^{1-r}$ for all $\kappa \neq \kappa_1$, but $\Pr_A\left(\kappa_1\right) = 0$, then $\Delta_{N;aa1,B}\left(r\right) \to \infty$. However, $\Pr_A\left(\kappa_1\right) = 0$ also implies that the density matrix coefficients involving a are strictly zero, so we need not worry about this case.

We note that for each κ, the variable r has a closed interval I_κ, containing p_κ in its interior, such that $p^r_\kappa\left(1-p_\kappa\right)^{1-r} \geq p^r_{\kappa'}\left(1-p_{\kappa'}\right)^{1-r}$ for all $\kappa' \neq \kappa$ (i.e. I_κ satisfies (i) in its interior and (ii) at its endpoints). We say that r is congruous with $\mathcal{C}_\kappa$ in this interval I_κ (and congruous to two different $\mathcal{C}_\kappa$ at the intersecting endpoints of such intervals).

For arbitrary (in particular, the "off-diagonal") terms, the positivity condition combined with Eq. (3.47) as $N \to \infty$ tells us that we must have $\Delta_{N;aa'e,B}\left(r\right) \to 0$, except when r is congruous with both a and a', in which case $\left|\Delta_{N;aa'e,B}\left(r\right)\right| \leq \Delta_{N;aa1,B}\left(r\right)$, and $\Delta_{N;aa'e,B}\left(r\right) \to \infty$ should not be allowed (except when the density matrix elements involving a or a' are strictly zero, making it irrelevant). From

this we find that either:

(a) there is some κ (possibly even with a and/or a' in $\mathcal{C}_\kappa$) with $\Pr_A(\kappa) \neq 0$ and $p_\kappa^r (1-p_\kappa)^{1-r} > \left| p^{\rightarrow}_{aa'e,B} \right|^r \left| p^{\uparrow}_{aa'e,B} \right|^{1-r}$, in which case $\Delta_{N;aa'e,B}(r) \to 0$, or

(b) $\left| p^{\rightarrow}_{aa'e,B} \right|^r \left| p^{\uparrow}_{aa'e,B} \right|^{1-r} = \left(p^{\rightarrow}_{aa1,B} \right)^r \left(p^{\uparrow}_{aa1,B} \right)^{1-r} = \left(p^{\rightarrow}_{a'a'1,B} \right)^r \left(p^{\uparrow}_{a'a'1,B} \right)^{1-r}$ with r congruous with both a and a', in which case $|\Delta_{N;aa'e,B}(r)| \to \Delta_{N;aa1,B}(r)$.

Case (b) deserves some further inspection. First, we note that we have

$$\left| p^{\rightarrow}_{aa'e,B} \right|^r \left| p^{\uparrow}_{aa'e,B} \right|^{1-r} \leq p_\kappa^r (1-p_\kappa)^{1-r} \tag{3.48}$$

on the entire interval I_κ congruous with $a \in \mathcal{C}_\kappa$. If there is some point r_* in the interior of I_κ for which

$$\left| p^{\rightarrow}_{aa'e,B} \right|^{r_*} \left| p^{\uparrow}_{aa'e,B} \right|^{1-r_*} = p_\kappa^{r_*} (1-p_\kappa)^{1-r_*}, \tag{3.49}$$

then in order not to violate the inequality when r is increased or decreased from r_*, we must have

$$\frac{\left| p^{\rightarrow}_{aa'e,B} \right|}{\left| p^{\uparrow}_{aa'e,B} \right|} = \frac{p_\kappa}{1-p_\kappa}. \tag{3.50}$$

It follows that

$$\left| p^{\rightarrow}_{aa'e,B} \right|^r \left| p^{\uparrow}_{aa'e,B} \right|^{1-r} = p_\kappa^r (1-p_\kappa)^{1-r} \tag{3.51}$$

on the entire interval I_κ, and, more significantly, that

$$\left| p^{\rightarrow}_{aa'e,B} \right| = 1 - \left| p^{\uparrow}_{aa'e,B} \right| = p_\kappa. \tag{3.52}$$

The same argument holds with respect to a' instead of a, giving the additional condition $a, a' \in \mathcal{C}_\kappa$. Hence, even at exponentially suppressed r, superpositions of anyonic charges from different $\mathcal{C}_\kappa$ do not survive measurement.

Pushing this a bit further, we note that for $r \in [0,1]$ and fixed $p \in [0,1]$

$$r^r (1-r)^{1-r} \geq p^r (1-p)^{1-r} \tag{3.53}$$

with equality at $r = p$. The positivity condition gave us (rewriting (a) and (b))

$$\max_\kappa \left\{ p_\kappa^r (1-p_\kappa)^{1-r} \right\} \geq \left| p^{\rightarrow}_{aa'e,B} \right|^r \left| p^{\uparrow}_{aa'e,B} \right|^{1-r} \tag{3.54}$$

with equality for $r \in I_\kappa$ if $a, a' \in \mathcal{C}_\kappa$ and $\left| p^{\rightarrow}_{aa'e,B} \right| = 1 - \left| p^{\uparrow}_{aa'e,B} \right| = p_\kappa$. Combining these, we have

$$r^r (1-r)^{1-r} \geq \left| p^{\rightarrow}_{aa'e,B} \right|^r \left| p^{\uparrow}_{aa'e,B} \right|^{1-r} \tag{3.55}$$

for all r, with equality occurring at $r = \left| p^{\rightarrow}_{aa'e,B} \right|$ only when $p_a = p_{a'} = \left| p^{\rightarrow}_{aa'e,B} \right| = 1 - \left| p^{\uparrow}_{aa'e,B} \right|$. If $\left| p^{\rightarrow}_{aa'e,B} \right| + \left| p^{\uparrow}_{aa'e,B} \right| > 1$, then there is some r (e.g. $r = \left| p^{\rightarrow}_{aa'e,B} \right|$)

for which $r^r\,(1-r)^{1-r} < \left|\,p^{\rightarrow}_{aa'e,B}\right|^r \left|p^{\uparrow}_{aa'e,B}\right|^{1-r}$, violating Eq. (3.55). If $\left|\,p^{\rightarrow}_{aa'e,B}\right| + \left|p^{\uparrow}_{aa'e,B}\right| = 1$, then $r^r\,(1-r)^{1-r} = \left|\,p^{\rightarrow}_{aa'e,B}\right|^r \left|p^{\uparrow}_{aa'e,B}\right|^{1-r}$ at $r = \left|\,p^{\rightarrow}_{aa'e,B}\right|$. Hence, we have

$$\left|\,p^{\rightarrow}_{aa'e,B}\right| + \left|p^{\uparrow}_{aa'e,B}\right| \leq 1 \tag{3.56}$$

with equality only if $p_a = p_{a'} = \left|\,p^{\rightarrow}_{aa'e,B}\right| = 1 - \left|p^{\uparrow}_{aa'e,B}\right|$. We believe one should be able to to show that this condition on $p^{s}_{aa'e,b}$ follows directly from the properties of anyon models, in which case these arguments could be made in the opposite direction, i.e. that positivity of the density matrix being preserved by these probe measurements follows from properties of anyon models; however, we have been unable to succeed in doing so.

For $p^{\rightarrow}_{aa'e,B} = p_\kappa e^{i\alpha_{aa'e,B}}$ and $p^{\uparrow}_{aa'e,B} = (1-p_k)\,e^{i\beta_{aa'e,B}}$, we see that if $\alpha_{aa'e,B} = \beta_{aa'e,B}$, then

$$|t_1|^2\,M_{eB} + |r_1|^2 = p^{\rightarrow}_{aa'e,B} + p^{\uparrow}_{aa'e,B} = e^{i\alpha_{aa'e,B}} \tag{3.57}$$

implies that either: (a) $r_1 = 0$ and $M_{eB} = e^{i\alpha_{aa'e,B}}$, or (b) $M_{eB} = 1$ and $\alpha_{aa'e,B} = \beta_{aa'e,B} = 0$.

One might also find it instructive to consider a large N expansion (using Stirling's formula) around p_κ to get

$$w_N\left(r; p^{\rightarrow}_{aa'e,B}, p^{\uparrow}_{aa'e,B}\right) \simeq w_N\left(r; p_\kappa, 1-p_\kappa\right) e^{-G_N\left(r; p^{\rightarrow}_{aa'e,B}, p^{\uparrow}_{aa'e,B}\right)} \tag{3.58}$$

$$\Delta_{N;aa'e,B}\left(r\right) \simeq \frac{1}{\Pr_A\left(\kappa\right)} e^{-G_N\left(r; p^{\rightarrow}_{aa'e,B}, p^{\uparrow}_{aa'e,B}\right)} \tag{3.59}$$

$$\begin{aligned} G_N\left(r;p,q\right) \approx & N\left[p_\kappa \ln\left(\frac{p_\kappa}{p}\right) + \left(1-p_\kappa\right)\ln\left(\frac{1-p_\kappa}{q}\right)\right] \\ & + N\left(r-p_\kappa\right)\ln\left(\frac{p_\kappa}{p}\frac{q}{\left(1-p_\kappa\right)}\right). \end{aligned} \tag{3.60}$$

Clearly, $e^{-G_N(r;p,q)}$ gives exponential suppression in N, unless $p = p_\kappa e^{i\alpha}$ and $q = (1-p_k)\,e^{i\beta}$, in which case

$$e^{-G_N(r;p,q)} = e^{i[\alpha p_\kappa + \beta(1-p_\kappa)]N} e^{i(\alpha-\beta)N(r-p_\kappa)} \tag{3.61}$$

(which is equal to 1, when $\alpha = \beta = 0$). We also note that integrating the quantity $w_N\left(r; p^{\rightarrow}_{aa'e,B}, p^{\uparrow}_{aa'e,B}\right)$ over r vanishes exponentially in N, unless $\alpha_{aa'e,B} = \beta_{aa'e,B} = 0$, which is why such quasi-fixed terms do not appear in Eq. (3.29), the density matrix obtained by ignoring measurement outcomes (except in the case when $r_1 = 0$).

To summarize, we found that, for large N, the quantity $\Delta_{N;aa'e,B}\left(r\right)$ vanishes exponentially unless r is congruous with $a, a' \in \mathcal{C}_\kappa$ and $\left|\,p^{\rightarrow}_{aa'e,B}\right| = 1 - \left|p^{\uparrow}_{aa'e,B}\right| = p_\kappa$.

This means a measurement outcome fraction r exponentially collapses the density matrix onto one that has support only in $\mathcal{C}_\kappa$, and consequently will drive r toward p_κ. The resulting target anyon reduced density matrix

$$\rho^A(r) = \sum_{\substack{a,a',c,c',f,\mu,\mu' \\ e,\alpha,\beta,f',\nu,\nu'}} \frac{\rho^A_{(a,c;f,\mu)(a',c';f,\mu')}}{(d_f d_{f'})^{1/2}} \Delta_{aa'e,B}(r) \times \left[(F^{ac}_{a'c'})^{-1}\right]_{(f,\mu,\mu')(e,\alpha,\beta)} \left[F^{ac}_{a'c'}\right]_{(e,\alpha,\beta)(f',\nu,\nu')} |a,c;f',\nu\rangle \langle a',c';f',\nu'|, \quad (3.62)$$

where

$$\Delta_{aa'e,B}(r) = \lim_{N\to\infty} \Delta_{N;aa'e,B}(r), \quad (3.63)$$

is found with the probability distribution

$$\Pr(r) = \sum_\kappa \Pr_A(\kappa)\, \delta(r - p_\kappa). \quad (3.64)$$

The resulting density matrices are of two forms:

(1) ***fixed states***, for which all non-zero elements of the density matrix correspond to $p^{\rightarrow}_{aa'e,B} = 1 - p^{\uparrow}_{aa'e,B} = p_\kappa$, and

(2) *rogues states* (or *quasi-fixed states*), for which all elements of the density matrix correspond to $\left|p^{\rightarrow}_{aa'e,B}\right| = 1 - \left|p^{\uparrow}_{aa'e,B}\right| = p_\kappa$, but for some of the "off-diagonal" elements ($e \neq 1$) with $p^{\rightarrow}_{aa'e,B} = p_\kappa e^{i\alpha_{aa'e,B}}$ and $p^{\uparrow}_{aa'e,B} = (1-p_k)\, e^{i\beta_{aa'e,B}}$, where $\alpha_{aa'e,B}$ and $\beta_{aa'e,B}$ are non-zero (unless $r_1 = 0$).

Fixed states have the property that probe measurements leave their density matrix invariant. Rogue states have the property that probe measurements leave their "diagonal" elements and possibly some of their "off-diagonal" elements invariant, while some of their "off-diagonal" elements are unchanged in magnitude, but have a changing phase. We will see in Section 3.2.2 that satisfying the conditions for rogue states requires non-generic experimental parameters.

3.2.2 Minding our p's

In Section 3.2.1, we have shown that performing many probe measurements collapses the target density matrix onto its elements which correspond to $p^s_{aa'e,B}$ satisfying

$$\left|p^{\rightarrow}_{aa'e,B}\right| = 1 - \left|p^{\uparrow}_{aa'e,B}\right| = p_\kappa \quad (3.65)$$

for $a, a' \in \mathcal{C}_\kappa$, so we would like to determine when this condition is satisfied.

For completeness, we first list the results for the trivial cases where there is no actual interferometry (for which $\mathcal{C}_1 = \mathcal{C}$):

(i) When $t_1 = 0$, we have $p^{\rightarrow}_{aa'e,B} = |t_2|^2$ and $p^{\uparrow}_{aa'e,B} = |r_2|^2$, so all elements are fixed.

(ii) When $r_1 = 0$, we have $p^{\rightarrow}_{aa'e,B} = |r_2|^2 M_{eB}$ and $p^{\uparrow}_{aa'e,B} = |t_2|^2 M_{eB}$, so elements with $M_{eB} = e^{i\varphi_{eB}}$ ($\varphi_{eB} \neq 0$) are quasi-fixed, and those with $M_{eB} = 1$ are fixed.

(iii) When $t_2 = 0$ (and $t_1 \neq 0$), we have $p^{\rightarrow}_{aa'e,B} = |t_1|^2 M_{eB}$ and $p^{\uparrow}_{aa'e,B} = |r_1|^2$, so elements with $M_{eB} = e^{i\varphi_{eB}}$ ($\varphi_{eB} \neq 0$) are quasi-fixed, and those with $M_{eB} = 1$ are fixed.

(iv) When $r_2 = 0$ (and $t_1 \neq 0$), we have $p^{\rightarrow}_{aa'e,B} = |r_1|^2$ and $p^{\uparrow}_{aa'e,B} = |t_1|^2 M_{eB}$, so elements with $M_{eB} = e^{i\varphi_{eB}}$ ($\varphi_{eB} \neq 0$) are quasi-fixed, and those with $M_{eB} = 1$ are fixed.

From here on, we assume that $|t_1 r_1 t_2 r_2| \neq 0$ (unless explicitly stated otherwise). We begin by considering the more stringent condition necessary for fixed elements. Using $p^{\rightarrow}_{aa'e,b} + p^{\uparrow}_{aa'e,b} = |t_1|^2 M_{eB} + |r_1|^2$, and Eq. (2.40), we have:

(v) (When $t_1 \neq 0$) An element is fixed, with $p^{\rightarrow}_{aa'e,b} = 1 - p^{\uparrow}_{aa'e,b} = p_\kappa$, iff $M_{eB} = 1$, and this implies $M_{aB} = M_{a'B}$ and $a, a' \in \mathcal{C}_\kappa$.

Thus, even without initially requiring $a, a' \in \mathcal{C}_\kappa$ (from positivity), we find that it is a necessary condition for fixed elements.

Now, we examine the conditions that give quasi-fixed elements. Such terms have $p^{\rightarrow}_{aa'e,B} = p_\kappa e^{i\alpha_{aa'e,B}}$ and $p^{\uparrow}_{aa'e,B} = (1-p_\kappa)\, e^{i\beta_{aa'e,B}}$, with $\alpha_{aa'e,B} \neq \beta_{aa'e,B}$ and $a, a' \in \mathcal{C}_\kappa$. (Recall that if $\alpha_{aa'e,B} = \beta_{aa'e,B}$ and $r_1 \neq 0$, then $\alpha_{aa'e,B} = \beta_{aa'e,B} = 0$.) Examining these conditions for $M_{aB} = M_{a'B}$, we find

$$\begin{aligned} 0 &= |t_2|^2 \left(\left| p^{\rightarrow}_{aa'e,B} \right|^2 - p_\kappa^2 \right) + |r_2|^2 \left(\left| p^{\uparrow}_{aa'e,B} \right|^2 - (1-p_\kappa)^2 \right) \\ &= |t_1|^4 |t_2|^2 |r_2|^2 \left(|M_{eB}|^2 - 1 \right) \\ &\quad + 2 |t_1|^2 |r_1|^2 |t_2|^2 |r_2|^2 \left(\mathrm{Re}\left\{ M_{eB} \right\} - 1 \right) \end{aligned} \tag{3.66}$$

which requires $M_{eB} = 1$ and, hence, gives us:

(vi) (When $|t_1 r_1 t_2 r_2| \neq 0$) There are no quasi-fixed elements for $p^s_{aa'e,B}$ with $M_{aB} = M_{a'B}$, only fixed ones. (In particular, this applies to $a = a'$.)

For $M_{aB} \neq M_{a'B}$, we can only have $a, a' \in \mathcal{C}_\kappa$ (i.e. $p^s_{aa1,B} = p^s_{a'a'1,B}$) when the experimental parameters are tuned to $\theta = -\arg\left\{ M_{aB} - M_{a'B} \right\} \pm \frac{\pi}{2}$, so quasi-fixed elements only occur non-generically. From the conditions on $p^s_{aa'e,B}$, at these values of θ, we find

$$
\begin{aligned}
0 &= \left|p^{\rightarrow}_{aa'e,B}\right|^2 - p_\kappa^2 - \left|p^{\uparrow}_{aa'e,B}\right|^2 + (1-p_\kappa)^2 \\
&= |t_1|^4 \left(|t_2|^2 - |r_2|^2\right)\left(1 - |M_{eB}|^2\right) \\
&\quad -2\,|t_1|^2 \left(1 - \text{Re}\left\{M_{eB}\right\}\right) 2\,|t_1 r_1 t_2 r_2| \,\text{Re}\left\{e^{i\theta} M_{aB}\right\} \\
&\quad +2\,|t_1|^2 \,\text{Im}\left\{M_{eB}\right\} |t_1 r_1 t_2 r_2| \,\text{Im}\left\{e^{i\theta} M_{aB} + e^{-i\theta} M^*_{a'B}\right\}
\end{aligned} \tag{3.67}
$$

and

$$
\begin{aligned}
0 &= |t_2|^2 \left(\left|p^{\rightarrow}_{aa'e,B}\right|^2 - p_\kappa^2\right) + |r_2|^2 \left(\left|p^{\uparrow}_{aa'e,B}\right|^2 - (1-p_\kappa)^2\right) \\
&= |t_1|^4 |t_2|^2 |r_2|^2 \left(|M_{eB}|^2 - 1\right) + 2\,|t_1|^2 |r_1|^2 |t_2|^2 |r_2|^2 \left(\text{Re}\left\{M_{eB}\right\} - 1\right) \\
&\quad + \left(|t_1 r_1 t_2 r_2| \,\text{Im}\left\{e^{i\theta} M_{aB} + e^{-i\theta} M^*_{a'B}\right\}\right)^2
\end{aligned} \tag{3.68}
$$

which may be rewritten to give:

(vii) Quasi-fixed elements with $p^s_{aa'e,B}$ only occur non-generically, and the conditions (when $|t_1 r_1 t_2 r_2| \neq 0$) that must be satisfied for them to occur are:

$$
\theta = -\arg\left\{M_{aB} - M_{a'B}\right\} \pm \frac{\pi}{2} \tag{3.69}
$$

$$
\left[\text{Im}\left\{e^{i\theta} M_{aB} + e^{-i\theta} M^*_{a'B}\right\}\right]^2 = \frac{|t_1|^2}{|r_1|^2}\left(1 - |M_{eB}|^2\right) + 2\left(1 - \text{Re}\left\{M_{eB}\right\}\right) \tag{3.70}
$$

$$
\begin{aligned}
&\text{Re}\left\{e^{i\theta} M_{aB}\right\} = \left[\frac{|t_1|}{4\,|r_1|}\left(\frac{|t_2|}{|r_2|} - \frac{|r_2|}{|t_2|}\right)\left(1 - |M_{eB}|^2\right)\right. \\
&\left. + \frac{1}{2}\text{Im}\left\{M_{eB}\right\} \text{Im}\left\{e^{i\theta} M_{aB} + e^{-i\theta} M^*_{a'B}\right\}\right] \left(1 - \text{Re}\left\{M_{eB}\right\}\right)^{-1}.
\end{aligned} \tag{3.71}
$$

To demonstrate that it is, in fact, sometimes possible to satisfy the conditions for quasi-fixed elements given in (vii), we present the following example:

Consider an anyon model which has at least two different Abelian anyons a and a', and some anyon b for which $M_{ab} = e^{i\varphi_{ab}}$ and $M_{a'b} = e^{i\varphi_{a'b}}$ are not equal (for example, almost any $\mathbb{Z}_N$ model, such as $\mathbb{Z}_2^{(1/2)}$ or $\mathbb{Z}_3^{(1)}$, is sufficient). The difference charge e is uniquely determined (since a and a' are Abelian) and has $M_{eb} = e^{i\varphi_{eb}} = e^{i(\varphi_{ab} - \varphi_{a'b})}$. Setting $\theta = -\frac{1}{2}\left(\varphi_{ab} + \varphi_{a'b}\right) + n\pi$ gives

$$p^{\rightarrow}_{aa'e,b} = \left(|t_1|\,|r_2|\,e^{i\left(\frac{\varphi_{eb}}{2}+n\pi\right)} + |r_1|\,|t_2| \right)^2 \tag{3.72}$$

$$p^{\uparrow}_{aa'e,b} = \left(-|t_1|\,|t_2|\,e^{i\left(\frac{\varphi_{eb}}{2}+n\pi\right)} + |r_1|\,|r_2| \right)^2 \tag{3.73}$$

$$\begin{aligned} p^{\rightarrow}_{aa1,b} &= p^{\rightarrow}_{a'a'1,b} = \left| p^{\rightarrow}_{aa'e,b} \right| = 1 - \left| p^{\uparrow}_{aa'e,b} \right| \\ &= |t_1|^2\,|r_2|^2 + 2\,|t_1 r_1 t_2 r_2| \cos\left(\frac{\varphi_{eb}}{2} + n\pi\right) + |r_1|^2\,|t_2|^2 . \end{aligned} \tag{3.74}$$

In fact, it turns out this example is the only way to satisfy the conditions for quasi-fixed elements with $|M_{eB}| = 1$. Indeed, this can even be shown without initially requiring $a, a' \in \mathcal{C}_\kappa$ from positivity. It seems rather difficult to satisfy the conditions for quasi-fixed elements when $|M_{eB}| \neq 1$, and we suspect (but are unable to prove) that it may, in general, actually be impossible. It is certainly not possible to have quasi-fixed elements with $|M_{eB}| \neq 1$ for arbitrary non-Abelian anyon models, as one can check that they do not exist for either the Ising or Fib anyon models, for example.

3.3 Distinguishability

We would like to know how many probe anyons should be used to establish a desired level of confidence in distinguishing between the various possible outcomes. For a confidence level $1-\alpha$, the margin of error around p_κ is specified as

$$E_\kappa = z^*_{\alpha/2}\sigma_\kappa, \tag{3.75}$$

i.e. the interval $[p_\kappa - E_\kappa, p_\kappa + E_\kappa]$ contains $1-\alpha$ of the probability distribution, where $z^*_{\alpha/2}$ is defined by

$$1 - \alpha = \text{erf}\left(\frac{z^*_{\alpha/2}}{\sqrt{2}}\right). \tag{3.76}$$

To achieve this level of confidence in distinguishing two values, p_1 and p_2, we pick N so that these intervals have no overlap

$$\begin{aligned} \Delta p = |p_1 - p_2| \gtrsim E_1 + E_2 &= z^*_{\alpha/2}\left(\sigma_1 + \sigma_2\right) \\ &= z^*_{\alpha/2}\left(\sqrt{\frac{p_1\left(1-p_1\right)}{N}} + \sqrt{\frac{p_2\left(1-p_2\right)}{N}} \right) \end{aligned} \tag{3.77}$$

which gives the estimated number of probes needed as

$$N \gtrsim \left(\frac{z^*_{\alpha/2}\left(\sqrt{p_1\left(1-p_1\right)} + \sqrt{p_2\left(1-p_2\right)} \right)}{\Delta p} \right)^2 . \tag{3.78}$$

Since $p\,(1-p) \leq \frac{1}{4}$, we could conservatively estimate this for arbitrary p_j as

$$N \gtrsim \left(\frac{z^*_{\alpha/2}}{\Delta p}\right)^2. \tag{3.79}$$

On the other hand, if p_1 and p_2 are of order $|t_1|^2 \sim |t_2|^2 \sim t^2 \ll 1$, and Δp is of order $2t^2\Delta M$, where $\Delta M = |M_{a_1 B} - M_{a_2 B}|$, (i.e. employing θ such that Δp is as large as it can be) then we can estimate

$$N \gtrsim \left(\frac{z^*_{\alpha/2}}{t\Delta M}\right)^2. \tag{3.80}$$

We note that for any two outcome probabilities, p_1 and p_2, there are always two values of θ (i.e. non-generic conditions) that make $p_1 = p_2$, and hence indistinguishable. Here are the values of $z^*_{\alpha/2}$ for some typical levels of confidence

$1-\alpha$	.6827	.9545	.99	.999	.9999
$z^*_{\alpha/2}$	1	2	2.576	3.2905	3.89059

For greater confidence, the number of probes needed roughly scales as $N \sim -\log \alpha$.

A special case of interest exists when $|t_1| = |t_2|$ and $|M_{a_1 B}| = 1$ for one of two probabilities that we wish to distinguish. In this case, using $\theta = \pi - \arg\{M_{a_1 B}\}$ gives $p_1 = 0$, so any measurement outcome $s = \!\!\rightarrow$ automatically tells us the target's anyonic charge is not in $\mathcal{C}_1$. If the alternative outcome has $p_2 \neq 0, 1$, then $\mathcal{C}_1$ and $\mathcal{C}_2$ are said to be sometimes perfectly distinguishable, since a $s = \!\!\rightarrow$ outcomes tells us the target's anyonic charge is in $\mathcal{C}_2$. If $M_{a_1 B} = -M_{a_2 B}$ and we also have $|t_j|^2 = 1/2$, then $p_2 = 1$, and $\mathcal{C}_1$ and $\mathcal{C}_2$ are always perfectly distinguishable, since any single probe measurement will indicate whether the target's anyonic charge is in $\mathcal{C}_1$ or in $\mathcal{C}_2$.

3.4 Target System Configuration

In this section, we consider the effect of locating the anyons C that are entangled with the target A in different regions outside the central interferometry region. If C is located above the central interferometer region, we would have

$$V = \begin{bmatrix} R_{BC} & 0 \\ 0 & R_{BC} \end{bmatrix}, \tag{3.81}$$

for which similar diagrammatic evaluation gives

$$p^{\rightarrow}_{aa'e,B} = |t_1|^2 |r_2|^2 + t_1 r_1^* r_2^* t_2^* e^{i(\theta_{\mathrm{I}}-\theta_{\mathrm{II}})} M_{a'B} + t_1^* r_1 t_2 r_2 e^{-i(\theta_{\mathrm{I}}-\theta_{\mathrm{II}})} M^*_{aB} + |r_1|^2 |t_2|^2 M^*_{eB}, \tag{3.82}$$

$$p^{\uparrow}_{aa'e,B} = |t_1|^2 |t_2|^2 - t_1 r_1^* r_2^* t_2^* e^{i(\theta_{\mathrm{I}}-\theta_{\mathrm{II}})} M_{a'B} - t_1^* r_1 t_2 r_2 e^{-i(\theta_{\mathrm{I}}-\theta_{\mathrm{II}})} M^*_{aB} + |r_1|^2 |r_2|^2 M^*_{eB}. \tag{3.83}$$

instead of Eqs. (3.14,3.15,3.21). If C is located between the output legs of the interferometer, we would instead have

$$V = \begin{bmatrix} R_{BC} & 0 \\ 0 & R^{-1}_{CB} \end{bmatrix}. \tag{3.84}$$

The resulting diagrammatic evaluation in this case gives

$$p^{\rightarrow}_{aa'e,B} = |t_1|^2 |r_2|^2 + t_1 r_1^* r_2^* t_2^* e^{i(\theta_{\mathrm{I}}-\theta_{\mathrm{II}})} M_{a'B} + t_1^* r_1 t_2 r_2 e^{-i(\theta_{\mathrm{I}}-\theta_{\mathrm{II}})} M^*_{aB} + |r_1|^2 |t_2|^2 M^*_{eB}, \tag{3.85}$$

$$p^{\uparrow}_{aa'e,B} = |t_1|^2 |t_2|^2 M_{eB} - t_1 r_1^* r_2^* t_2^* e^{i(\theta_{\mathrm{I}}-\theta_{\mathrm{II}})} M_{aB} - t_1^* r_1 t_2 r_2 e^{-i(\theta_{\mathrm{I}}-\theta_{\mathrm{II}})} M^*_{a'B} + |r_1|^2 |r_2|^2. \tag{3.86}$$

For both of these cases, the arguments from before apply directly and limiting behavior is exactly the same. One can also envision more complicated situations, such as having the C anyons distributed amongst all the regions outside the central one. The resulting calculations are straightforward, but too cumbersome to display here explicitly. However, the limiting behavior is essentially the same as before, as one would expect from the previous analysis: Interferometry measurement generically collapses the target system onto fixed states, which are characterized as having the target anyons A (those which the probes interfere around) in a charge subset that the probe cannot distinguish by monodromy (i.e. a, a' such that $M_{aB} = M_{a'b}$), and the anyons in distinct regions having no coherent anyonic charge entanglement crossing the probe anyons' beam paths that the probes can "see" by monodromy (i.e. anyonic charge entanglement characterized by charge e can entangle anyons in distinct regions only if $M_{eB} = 1$).

3.5 Probe Generalizations

In this section, we examine the effects of using probe systems that are even more general than those employed so far. We will first consider generalizing the input direction, so that probes may enter in arbitrary superpositions of the two input directions. Then we will consider the use of probes that are not identical, so that each probe system is described by a different density matrix. For both of these, the probe systems and target system are all still initially unentangled. One may also consider

cases where there is nontrivial initial entanglement between these systems, or post-interferometer charge projections, but these typically lead to qualitatively different behavior, and greatly increase the complexity of analysis, so we will not consider them here.

3.5.1 Generalized Input Directions

For probes that are allowed to enter the interferometer through either of the input legs, possibly even in superposition, the probe systems' density matrices take the form

$$\rho^B = \sum_{b,b',d,d',h,\lambda,\lambda',r,r'} \rho^B_{(d,b_r;h,\lambda)(d',b'_{r'};h,\lambda')} \frac{1}{d_h} \left|d, b_r; h, \lambda\right\rangle \left\langle d', b'_{r'}; h, \lambda'\right| . \tag{3.87}$$

Using this, we find the same result as before, except, instead of Eqs. (3.14,3.15,3.21), the values of $p^s_{aa'e,B}$ are given by

$$p^s_{aa'e,B} = \sum_{d,h,\lambda,b,r,r'} \rho^B_{(d,b_r;h,\lambda)(d,b_{r'};h,\lambda)} p^s_{aa'e,b,r,r'} \tag{3.88}$$

where

$$\begin{aligned}
p^{\rightarrow}_{aa'e,b,\rightarrow,\rightarrow} &= |t_1|^2 |r_2|^2 M_{eb} + t_1 r_1^* t_2^* r_2^* e^{i(\theta_{\rm I}-\theta_{\rm II})} M_{ab} \\
&\quad + t_1^* r_1 t_2 r_2 e^{-i(\theta_{\rm I}-\theta_{\rm II})} M^*_{a'b} + |r_1|^2 |t_2|^2 && (3.89)\\
p^{\rightarrow}_{aa'e,b,\rightarrow,\uparrow} &= t_1 r_1 |r_2|^2 M_{eb} - t_1 t_1 t_2^* r_2^* e^{i(\theta_{\rm I}-\theta_{\rm II})} M_{ab} \\
&\quad + r_1 r_1 t_2 r_2 e^{-i(\theta_{\rm I}-\theta_{\rm II})} M^*_{a'b} - t_1 r_1 |t_2|^2 && (3.90)\\
p^{\rightarrow}_{aa'e,b,\uparrow,\rightarrow} &= t_1^* r_1^* |r_2|^2 M_{eb} + r_1^* r_1^* t_2^* r_2^* e^{i(\theta_{\rm I}-\theta_{\rm II})} M_{ab} \\
&\quad - t_1^* t_1^* t_2 r_2 e^{-i(\theta_{\rm I}-\theta_{\rm II})} M^*_{a'b} - t_1^* r_1^* |t_2|^2 && (3.91)\\
p^{\rightarrow}_{aa'e,b,\uparrow,\uparrow} &= |r_1|^2 |r_2|^2 M_{eb} - t_1 r_1^* t_2^* r_2^* e^{i(\theta_{\rm I}-\theta_{\rm II})} M_{ab} \\
&\quad - t_1^* r_1 t_2 r_2 e^{-i(\theta_{\rm I}-\theta_{\rm II})} M^*_{a'b} + |t_1|^2 |t_2|^2 && (3.92)
\end{aligned}$$

and

$$\begin{aligned}
p^{\uparrow}_{aa'e,b,\rightarrow,\rightarrow} &= |t_1|^2 |t_2|^2 M_{eb} - t_1 r_1^* t_2^* r_2^* e^{i(\theta_{\rm I}-\theta_{\rm II})} M_{ab} \\
&\quad - t_1^* r_1 t_2 r_2 e^{-i(\theta_{\rm I}-\theta_{\rm II})} M^*_{a'b} + |r_1|^2 |r_2|^2 && (3.93)\\
p^{\uparrow}_{aa'e,b,\rightarrow,\uparrow} &= t_1 r_1 |t_2|^2 M_{eb} + t_1 t_1 t_2^* r_2^* e^{i(\theta_{\rm I}-\theta_{\rm II})} M_{ab} \\
&\quad - r_1 r_1 t_2 r_2 e^{-i(\theta_{\rm I}-\theta_{\rm II})} M^*_{a'b} - t_1 r_1 |r_2|^2 && (3.94)\\
p^{\uparrow}_{aa'e,b,\uparrow,\rightarrow} &= t_1^* r_1^* |t_2|^2 M_{eb} - r_1^* r_1^* t_2^* r_2^* e^{i(\theta_{\rm I}-\theta_{\rm II})} M_{ab} \\
&\quad + t_1^* t_1^* t_2 r_2 e^{-i(\theta_{\rm I}-\theta_{\rm II})} M^*_{a'b} - t_1^* r_1^* |r_2|^2 && (3.95)\\
p^{\uparrow}_{aa'e,b,\uparrow,\uparrow} &= |r_1|^2 |t_2|^2 M_{eb} + t_1 r_1^* t_2^* r_2^* e^{i(\theta_{\rm I}-\theta_{\rm II})} M_{ab} \\
&\quad + t_1^* r_1 t_2 r_2 e^{-i(\theta_{\rm I}-\theta_{\rm II})} M^*_{a'b} + |t_1|^2 |r_2|^2 . && (3.96)
\end{aligned}$$

It is straightforward to check that

$$p^{\rightarrow}_{aa1,B} + p^{\uparrow}_{aa1,B} = \sum_{d,h,\lambda,b,r} \rho^{B}_{(d,b_r;h,\lambda)(d,b_r;h,\lambda)} = 1, \tag{3.97}$$

and one can see that, generically, the only terms in the target anyons' density matrix that will survive many probe measurements are those in e-channels with

$$M_{eB} = \sum_{d,h,\lambda,b,r} \rho^{B}_{(d,b_r;h,\lambda)(d,b_r;h,\lambda)} M_{eb} = 1. \tag{3.98}$$

3.5.2 Non-Identical Probes

When the probes $B_1, \ldots, B_N$ are described by different density matrices ρ^{B_j} (though are all still unentangled with each other and with the target system), we must use

$$p^{s}_{aa'e,B_j} = \sum_{b} \Pr{}_{B_j}(b)\, p^{s}_{aa'e,b} \tag{3.99}$$

$$\Pr{}_{B_j}(b) = \sum_{d,h,\lambda} \rho^{B_j}_{(d,b_\rightarrow;h,\lambda)(d,b_\rightarrow;h,\lambda)} \tag{3.100}$$

for each probe. This gives us the probability for the string of measurement outcomes $(s_1, \ldots, s_N)$ to occur as

$$\Pr(s_1, \ldots, s_N) = \sum_{a,c,f,\mu} \rho^{A}_{(a,c;f,\mu)(a,c;f,\mu)} p^{s_1}_{aa1,B_1} \cdots p^{s_N}_{aa1,B_N}, \tag{3.101}$$

with the resulting target anyon density matrix

$$\begin{aligned}\rho^{A}(s_1, \ldots, s_N) = &\sum_{\substack{a,a',c,c',f,\mu,\mu' \\ e,\alpha,\beta,f',\nu,\nu'}} \frac{\rho^{A}_{(a,c;f,\mu)(a',c';f,\mu')}}{(d_f d_{f'})^{1/2}} \frac{p^{s_1}_{aa'e,B_1} \cdots p^{s_N}_{aa'e,B_N}}{\Pr(s_1, \ldots, s_N)} \\ &\times \left[(F^{ac}_{a'c'})^{-1}\right]_{(f,\mu,\mu')(e,\alpha,\beta)} [F^{ac}_{a'c'}]_{(e,\alpha,\beta)(f',\nu,\nu')} |a, c; f', \nu\rangle \langle a', c'; f', \nu'|. \end{aligned} \tag{3.102}$$

With this generalization, we find that the order of measurement outcomes does, in fact, matter. This is obstructive to providing a quantitative description of the large N behavior; however, the qualitative behavior should be transparent after the analysis in previous sections for the identical probes. Each probe measurement will execute some amount of projection, to some extent collapsing superpositions of anyonic charges that the probe is able to distinguish by monodromy.

3.6 Examples

In this section, we apply the general results to some important examples, specifically: the $\mathbb{Z}_N$, Fibonacci, and Ising anyon models. (The application to some additional important examples, such as $\mathrm{SU}(2)_k$ and $\mathrm{D}(\mathbb{Z}_N)$, may be found in [79].) All of these have $N_{ab}^c = 0, 1$, so we will drop the fusion/splitting spaces' basis labels (greek indices), with the understanding that any symbol involving a prohibited fusion vertex is set to zero. Anyon models are completely specified by their F-symbols and R-symbols, so we will provide these, as well as list some additional important quantities that can be derived from them, for convenience. To relate these to interferometry experiments, we give the corresponding fixed state probabilities p_κ and density matrices ρ_κ^A, as described in Section 3.2.

3.6.1 $\mathbb{Z}_N^{(w)}$

The Abelian $\mathbb{Z}_N$ anyon models [8] have anyonic charges $\mathcal{C} = \{0, 1, \ldots, N-1\}$, where 0 here designates the vacuum charge. The fusion rules are just given by $\mathbb{Z}_N$ addition, and, to denote this, we define $[n]_N \in \mathcal{C}$ as the least residue of n mod N. The $\mathbb{Z}_N^{(w)}$ anyon models, where $w = n$ for N odd and $w = n$ and $n + \frac{1}{2}$ for N even, with $n = 0, 1, \ldots, N-1$, are described by:

<table>
<tr><td colspan="3">$\mathcal{C} = \{0, 1, \ldots, N-1\}, \quad a \times b = [a+b]_N$</td></tr>
<tr><td colspan="3">for $w = n$: $\left[F^{abc}_{[a+b+c]_N}\right]_{[a+b]_N[b+c]_N} = \left[F^{ab}_{c[a+b-c]_N}\right]_{[a-c]_N[a+b]_N} = 1$</td></tr>
<tr><td colspan="3">for $w = n + \frac{1}{2}$: $\left[F^{abc}_{[a+b+c]_N}\right]_{[a+b]_N[b+c]_N} = e^{i\frac{\pi}{N}a\left(b+c-[b+c]_N\right)}$,
$\left[F^{ab}_{c[a+b-c]_N}\right]_{[a-c]_N[a+b]_N} = e^{i\frac{\pi}{N}c\left([a-c]_N+b-[a+b-c]_N\right)}$</td></tr>
<tr><td>$R^{ab}_{[a+b]_N} = e^{i\frac{2\pi w}{N}ab}$</td><td>$S_{ab} = \frac{1}{\sqrt{N}}e^{i\frac{4\pi w}{N}ab}$</td><td>$M_{ab} = e^{i\frac{4\pi w}{N}ab}$</td></tr>
<tr><td colspan="2">$d_a = 1, \quad \mathcal{D} = \sqrt{N}$</td><td>$\theta_a = e^{i2\pi\frac{w}{N}a^2}$</td></tr>
</table>

These anyon models describe some Chern-Simons/WZW theories, e.g. $\mathrm{SU}(N)_1$, for which the corresponding anyon models are $\mathbb{Z}_N^{((N-1)/2)}$ for N odd and $\mathbb{Z}_N^{(N/2-1)}$ for N even; and $\mathrm{U}(1)_k$, for which the corresponding anyon models are $\mathbb{Z}_{2k}^{(1/2)}$ for $2k$ even and $\mathbb{Z}_{4k}^{(1)}$ for $2k$ odd.

Of course, for Abelian anyon models such as these, each physical quasiparticle excitation has a specific anyonic charge and all fusion channels are uniquely determined, so superpositions of anyonic charge are not actually possible, but such models might occur as a subset of a non-Abelian anyon model, in which case superpositions of these charges could potentially occur. In any case, one may still perform interferometry experiments in these models to determine the charge of a

target anyon. Using b probes, we have:

$$p_a = p^{\rightarrow}_{aa0,b} = |t_1|^2 |r_2|^2 + 2 |t_1 r_1 t_2 r_2| \cos\left(\theta + \frac{4\pi w}{N} ab\right) + |r_1|^2 |t_2|^2 \tag{3.103}$$

and

$$\Pr_A(\kappa) = \sum_{a \in C_\kappa, f} \rho_{(a,f-a;f)(a,f-a;f)} \tag{3.104}$$

$$\rho^A_\kappa = \sum_{a,a' \in C_\kappa, f} \frac{\rho_{(a,f-a;f)(a',f-a';f)}}{\Pr_A(\kappa)} |a, f-a; f\rangle \langle a', f-a'; f| \tag{3.105}$$

For $\mathbb{Z}_N^{(w)}$ with $\gcd(2w, N) = 1$ (i.e. the modular $\mathbb{Z}_N$ models), the charge classes are singletons $\mathcal{C}_a = \{a\}$, so $a = a'$ in the fixed state density matrices.

3.6.2 Fib

The Fibonacci (Fib) anyon model (also known as $\mathrm{SO}(3)_3$, since it may be obtained from the $\mathrm{SU}(2)_3$ anyon model by restricting to integer spins)[3] is known to be universal for topological quantum computation [86]. It has two charges $\mathcal{C} = \{1, \varepsilon\}$ and is described by (listing only the non-trivial F-symbols and R-symbols, i.e. those not listed are equal to one if their vertices are permitted by fusion, and equal to zero if they are not permitted):

$\mathcal{C} = \{1, \varepsilon\}, \quad 1 \times 1 = 1, \quad 1 \times \varepsilon = \varepsilon, \quad \varepsilon \times \varepsilon = 1 + \varepsilon$	
$[F^{\varepsilon\varepsilon\varepsilon}_\varepsilon]_{ef} = [F^{\varepsilon\varepsilon}_{\varepsilon\varepsilon}]_{ef} = \begin{bmatrix} \phi^{-1} & \phi^{-1/2} \\ \phi^{-1/2} & -\phi^{-1} \end{bmatrix}_{ef}$	
$R^{\varepsilon\varepsilon}_1 = e^{-i4\pi/5}, \quad R^{\varepsilon\varepsilon}_\varepsilon = e^{i3\pi/5}$	
$S = \frac{1}{\sqrt{\phi+2}} \begin{bmatrix} 1 & \phi \\ \phi & -1 \end{bmatrix}$	$M = \begin{bmatrix} 1 & 1 \\ 1 & -\phi^{-2} \end{bmatrix}$
$d_1 = 1, \quad d_\varepsilon = \phi, \quad \mathcal{D} = \sqrt{\phi+2}$	$\theta_1 = 1, \quad \theta_\varepsilon = e^{i\frac{4\pi}{5}}$

where $\phi = \frac{1+\sqrt{5}}{2}$ is the Golden ratio. We denote the anyon model given by this with the complex conjugate values of the R-symbols and topological spins as $\overline{\mathrm{Fib}}$.

For $b = \varepsilon$ probes, we have $\mathcal{C}_1 = \{1\}$, $\mathcal{C}_2 = \{\varepsilon\}$ and

$$p_1 = p^{\rightarrow}_{111,\varepsilon} = |t_1|^2 |r_2|^2 + 2 |t_1 r_1 t_2 r_2| \cos\theta + |r_1|^2 |t_2|^2 \tag{3.106}$$

$$p_2 = p^{\rightarrow}_{\varepsilon\varepsilon 1,\varepsilon} = |t_1|^2 |r_2|^2 - 2\phi^{-2} |t_1 r_1 t_2 r_2| \cos\theta + |r_1|^2 |t_2|^2 \tag{3.107}$$

[3] As a Chern-Simons or WZW theory, this is properly denoted as $\overline{(\mathrm{G}_2)_1}$, since $\mathrm{SO}(3)_k$ is only allowed for $k = 0 \bmod 4$.

$$\Pr_A(1) = \rho_{(1,1;1)(1,1;1)} + \rho_{(1,\varepsilon;\varepsilon)(1,\varepsilon;\varepsilon)} \tag{3.108}$$

$$\begin{aligned}\rho_1^A = \frac{1}{\Pr_A(1)} \Big\{ & \rho_{(1,1;1)(1,1;1)} |1,1;1\rangle \langle 1,1;1| \\ & + \phi^{-1} \rho_{(1,\varepsilon;\varepsilon)(1,\varepsilon;\varepsilon)} |1,\varepsilon;\varepsilon\rangle \langle 1,\varepsilon;\varepsilon| \Big\}\end{aligned} \tag{3.109}$$

$$\Pr_A(2) = \rho_{(\varepsilon,1;\varepsilon)(\varepsilon,1;\varepsilon)} + \rho_{(\varepsilon,\varepsilon;1)(\varepsilon,\varepsilon;1)} + \rho_{(\varepsilon,\varepsilon;\varepsilon)(\varepsilon,\varepsilon;\varepsilon)} \tag{3.110}$$

$$\begin{aligned}\rho_2^A = \frac{1}{\Pr_A(2)} \Big\{ & \phi^{-1} \rho_{(\varepsilon,1;\varepsilon)(\varepsilon,1;\varepsilon)} |\varepsilon,1;\varepsilon\rangle \langle \varepsilon,1;\varepsilon| \\ & + \phi^{-2} \left(\rho_{(\varepsilon,\varepsilon;1)(\varepsilon,\varepsilon;1)} + \rho_{(\varepsilon,\varepsilon;\varepsilon)(\varepsilon,\varepsilon;\varepsilon)} \right) \\ & \times \left[|\varepsilon,\varepsilon;1\rangle \langle \varepsilon,\varepsilon;1| + |\varepsilon,\varepsilon;\varepsilon\rangle \langle \varepsilon,\varepsilon;\varepsilon| \right] \Big\}\end{aligned} \tag{3.111}$$

We note that one can sometimes (approximately 69% of the time, when the target charge is not vacuum) perfectly distinguish the charges 1 and ε with a single $b = \varepsilon$ probe measurement by setting the experimental parameters to: $|t_1|^2 = |t_2|^2 = 1/2$ and $\theta = \pi$, which give $p_1 = 0$ and $p_2 = 1 - \frac{1}{2\phi} \simeq .69$.

3.6.3 Ising

The Ising anyon model is derived from the CFT that describes the Ising model at criticality [8]. It has anyonic charges $\mathcal{C} = \{1, \sigma, \psi\}$ (which respectively correspond to vacuum, spin, and Majorana fermions in the CFT). The anyon model is described by (listing only the non-trivial F-symbols and R-symbols):

<table>
<tr><td colspan="2">$\mathcal{C} = \{1, \sigma, \psi\}, \quad 1 \times a = a, \quad \sigma \times \sigma = 1 + \psi, \quad \sigma \times \psi = \sigma, \quad \psi \times \psi = 1$</td></tr>
<tr><td colspan="2">$[F_\sigma^{\sigma\sigma\sigma}]_{ef} = [F_{\sigma\sigma}^{\sigma\sigma}]_{ef} = \begin{bmatrix} \frac{1}{\sqrt{2}} & \frac{1}{\sqrt{2}} \\ \frac{1}{\sqrt{2}} & \frac{-1}{\sqrt{2}} \end{bmatrix}_{ef}$
$\left[F_\psi^{\sigma\psi\sigma}\right]_{\sigma\sigma} = \left[F_\sigma^{\psi\sigma\psi}\right]_{\sigma\sigma} = \left[F_{\psi\sigma}^{\sigma\psi}\right]_{\sigma\sigma} = \left[F_{\sigma\psi}^{\psi\sigma}\right]_{\sigma\sigma} = -1$</td></tr>
<tr><td colspan="2">$R_1^{\sigma\sigma} = e^{-i\frac{\pi}{8}}, \quad R_\psi^{\sigma\sigma} = e^{i\frac{3\pi}{8}}, \quad R_\sigma^{\sigma\psi} = R_\sigma^{\psi\sigma} = e^{-i\frac{\pi}{2}}, \quad R_1^{\psi\psi} = -1$</td></tr>
<tr><td>$S = \frac{1}{2} \begin{bmatrix} 1 & \sqrt{2} & 1 \\ \sqrt{2} & 0 & -\sqrt{2} \\ 1 & -\sqrt{2} & 1 \end{bmatrix}$</td><td>$M = \begin{bmatrix} 1 & 1 & 1 \\ 1 & 0 & -1 \\ 1 & -1 & 1 \end{bmatrix}$</td></tr>
<tr><td>$d_1 = d_\psi = 1, \quad d_\sigma = \sqrt{2}, \quad \mathcal{D} = 2$</td><td>$\theta_1 = 1, \quad \theta_\sigma = e^{i\frac{\pi}{8}}, \quad \theta_\psi = -1$</td></tr>
</table>

where $e, f \in \{1, \psi\}$.

For $b = \psi$ probes, we have $\mathcal{C}_1 = \{1, \psi\}$, $\mathcal{C}_2 = \{\sigma\}$, and

$$\begin{aligned} p_1 &= \vec{p_{111,\psi}} = \vec{p_{\psi\psi 1,\psi}} = \vec{p_{1\psi\psi,\psi}} = \vec{p_{\psi 1\psi,\psi}} \\ &= |t_1|^2 |r_2|^2 + 2 |t_1 r_1 r_2 t_2| \cos\theta + |r_1|^2 |t_2|^2 \end{aligned} \tag{3.112}$$

$$p_2 = \vec{p_{\sigma\sigma 1,\psi}} = \vec{p_{\sigma\sigma\psi,\psi}} = |t_1|^2 |r_2|^2 - 2 |t_1 r_1 r_2 t_2| \cos\theta + |r_1|^2 |t_2|^2 \tag{3.113}$$

$$\begin{aligned} \Pr_A(1) = &\rho_{(1,1;1)(1,1;1)} + \rho_{(1,\sigma;\sigma)(1,\sigma;\sigma)} + \rho_{(1,\psi;\psi)(1,\psi;\psi)} \\ &+\rho_{(\psi,1;\psi)(\psi,1;\psi)} + \rho_{(\psi,\sigma;\sigma)(\psi,\sigma;\sigma)} + \rho_{(\psi,\psi;1)(\psi,\psi;1)} \end{aligned} \tag{3.114}$$

$$\begin{aligned} \rho_1^A = \frac{1}{\Pr_A(1)} \Big\{ &\rho_{(1,1;1)(1,1;1)} |1,1;1\rangle \langle 1,1;1| + \rho_{(1,1;1)(\psi,\psi;1)} |1,1;1\rangle \langle \psi,\psi;1| \\ &+\rho_{(\psi,\psi;1)(1,1;1)} |\psi,\psi;1\rangle \langle 1,1;1| + \rho_{(\psi,\psi;1)(\psi,\psi;1)} |\psi,\psi;1\rangle \langle \psi,\psi;1| \\ +\frac{1}{\sqrt{2}} \Big(&\rho_{(1,\sigma;\sigma)(1,\sigma;\sigma)} |1,\sigma;\sigma\rangle \langle 1,\sigma;\sigma| + \rho_{(1,\sigma;\sigma)(\psi,\sigma;\sigma)} |1,\sigma;\sigma\rangle \langle \psi,\sigma;\sigma| \\ &+\rho_{(\psi,\sigma;\sigma)(1,\sigma;\sigma)} |\psi,\sigma;\sigma\rangle \langle 1,\sigma;\sigma| + \rho_{(\psi,\sigma;\sigma)(\psi,\sigma;\sigma)} |\psi,\sigma;\sigma\rangle \langle \psi,\sigma;\sigma| \Big) \\ +\rho_{(1,\psi;\psi)(1,\psi;\psi)} &|1,\psi;\psi\rangle \langle 1,\psi;\psi| + \rho_{(1,\psi;\psi)(\psi,1;\psi)} |1,\psi;\psi\rangle \langle \psi,1;\psi| \\ +\rho_{(\psi,1;\psi)(1,\psi;\psi)} &|\psi,1;\psi\rangle \langle 1,\psi;\psi| + \rho_{(\psi,1;\psi)(\psi,1;\psi)} |\psi,1;\psi\rangle \langle \psi,1;\psi| \Big\} \end{aligned} \tag{3.115}$$

$$\Pr_A(2) = \rho_{(\sigma,1;\sigma)(\sigma,1;\sigma)} + \rho_{(\sigma,\sigma;1)(\sigma,\sigma;1)} + \rho_{(\sigma,\sigma;\psi)(\sigma,\sigma;\psi)} + \rho_{(\sigma,\psi;\sigma)(\sigma,\psi;\sigma)} \tag{3.116}$$

$$\begin{aligned} \rho_2^A = \frac{1}{\Pr_A(2)} \Big\{ &\rho_{(\sigma,\sigma;1)(\sigma,\sigma;1)} |\sigma,\sigma;1\rangle \langle \sigma,\sigma;1| \\ +\frac{1}{\sqrt{2}} \Big(&\rho_{(\sigma,1;\sigma)(\sigma,1;\sigma)} |\sigma,1;\sigma\rangle \langle \sigma,1;\sigma| + \rho_{(\sigma,1;\sigma)(\sigma,\psi;\sigma)} |\sigma,1;\sigma\rangle \langle \sigma,\psi;\sigma| \\ +\rho_{(\sigma,\psi;\sigma)(\sigma,1;\sigma)} &|\sigma,\psi;\sigma\rangle \langle \sigma,1;\sigma| + \rho_{(\sigma,\psi;\sigma)(\sigma,\psi;\sigma)} |\sigma,\psi;\sigma\rangle \langle \sigma,1;\sigma| \Big) \\ &+\rho_{(\sigma,\sigma;\psi)(\sigma,\sigma;\psi)} |\sigma,\sigma;\psi\rangle \langle \sigma,\sigma;\psi| \Big\} \end{aligned} \tag{3.117}$$

For $b = \sigma$ probes, we have $\mathcal{C}_1 = \{1\}$, $\mathcal{C}_2 = \{\sigma\}$, $\mathcal{C}_3 = \{\psi\}$, and

$$p_1 = \vec{p_{111,\sigma}} = |t_1|^2 |r_2|^2 + 2 |t_1 r_1 r_2 t_2| \cos\theta + |r_1|^2 |t_2|^2 \tag{3.118}$$

$$p_2 = \vec{p_{\sigma\sigma 1,\sigma}} = |t_1|^2 |r_2|^2 + |r_1|^2 |t_2|^2 \tag{3.119}$$

$$p_3 = \vec{p_{\psi\psi 1,\sigma}} = |t_1|^2 |r_2|^2 - 2 |t_1 r_1 r_2 t_2| \cos\theta + |r_1|^2 |t_2|^2 \tag{3.120}$$

$$\Pr_A(1) = \rho_{(1,1;1)(1,1;1)} + \rho_{(1,\sigma;\sigma)(1,\sigma;\sigma)} + \rho_{(1,\psi;\psi)(1,\psi;\psi)} \tag{3.121}$$

$$\rho_1^A = \frac{1}{\Pr_A(1)} \Big\{ \rho_{(1,1;1)(1,1;1)} \left|1,1;1\right\rangle \left\langle 1,1;1\right| + \frac{1}{\sqrt{2}} \rho_{(1,\sigma;\sigma)(1,\sigma;\sigma)} \left|1,\sigma;\sigma\right\rangle \left\langle 1,\sigma;\sigma\right| + \rho_{(1,\psi;\psi)(1,\psi;\psi)} \left|1,\psi;\psi\right\rangle \left\langle 1,\psi;\psi\right| \Big\} \tag{3.122}$$

$$\Pr_A(2) = \rho_{(\sigma,1;\sigma)(\sigma,1;\sigma)} + \rho_{(\sigma,\sigma;1)(\sigma,\sigma;1)} + \rho_{(\sigma,\sigma;\psi)(\sigma,\sigma;\psi)} + \rho_{(\sigma,\psi;\sigma)(\sigma,\psi;\sigma)} \tag{3.123}$$

$$\rho_2^A = \frac{1}{\Pr_A(2)} \Bigg\{ \frac{1}{\sqrt{2}} \rho_{(\sigma,1;\sigma)(\sigma,1,\sigma)} \left|\sigma,1;\sigma\right\rangle \left\langle \sigma,1;\sigma\right| + \frac{1}{\sqrt{2}} \rho_{(\sigma,\psi;\sigma)(\sigma,\psi;\sigma)} \left|\sigma,\psi;\sigma\right\rangle \left\langle \sigma,\psi;\sigma\right| + \frac{1}{2} \left(\rho_{(\sigma,\sigma;1)(\sigma,\sigma;1)} + \rho_{(\sigma,\sigma;\psi)(\sigma,\sigma;\psi)} \right) \times \left[\left|\sigma,\sigma;1\right\rangle \left\langle \sigma,\sigma;1\right| + \left|\sigma,\sigma;\psi\right\rangle \left\langle \sigma,\sigma;\psi\right| \right] \Bigg\} \tag{3.124}$$

$$\Pr_A(3) = \rho_{(\psi,1;\psi)(\psi,1;\psi)} + \rho_{(\psi,\sigma;\sigma)(\psi,\sigma;\sigma)} + \rho_{(\psi,\psi;1)(\psi,\psi;1)} \tag{3.125}$$

$$\rho_3^A = \frac{1}{\Pr_A(3)} \Big\{ \rho_{(\psi,1;\psi)(\psi,1;\psi)} \left|\psi,1;\psi\right\rangle \left\langle \psi,1;\psi\right| + \frac{1}{\sqrt{2}} \rho_{(\psi,\sigma;\sigma)(\psi,\sigma;\sigma)} \left|\psi,\sigma;\sigma\right\rangle \left\langle \psi,\sigma;\sigma\right| + \rho_{(\psi,\psi;1)(\psi,\psi;1)} \left|\psi,\psi;1\right\rangle \left\langle \psi,\psi;1\right| \Big\} \tag{3.126}$$

We note that one can always perfectly distinguish the charges 1 and ψ with a single $b = \sigma$ probe measurement by setting the experimental parameters such that $|t_1|^2 = |t_2|^2 = 1/2$ and $\theta = \pi$, which give $p_1 = 0$ and $p_3 = 1$.

4 Fractional Quantum Hall Double Point-Contact Interferometer

After the detailed analysis of Section 3, one hopes that it has application in physical systems, and not just to the abstract idealizations that exist in our minds. In pursuing this hope, we turn our attention to fractional quantum Hall systems, since they represent the most likely candidates for possessing anyons and realizing braiding statistics of either Abelian or non-Abelian nature.

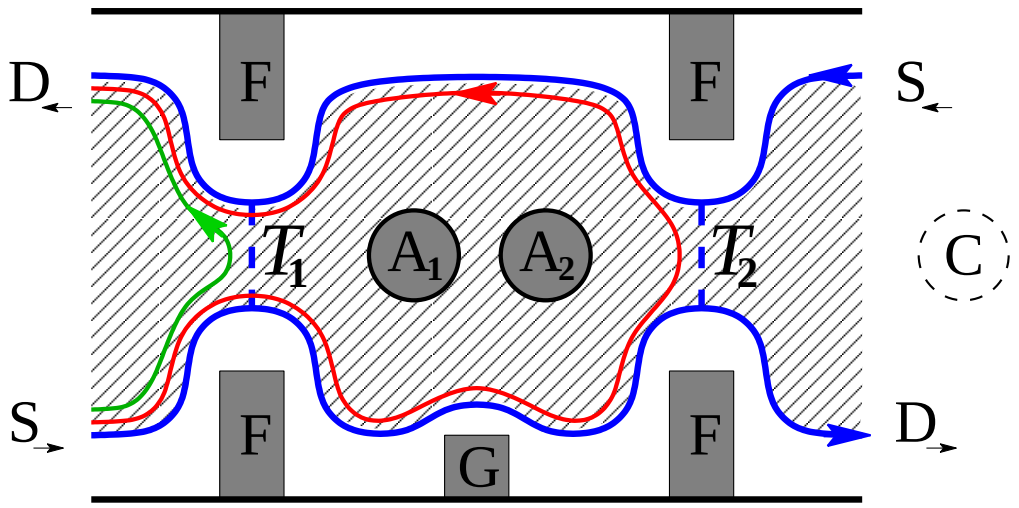

Fig. 3. A double point-contact interferometer for measuring braiding statistics in fractional quantum Hall systems. The hatched region contains an incompressible FQH liquid. S_s and D_s indicate the "sources" and "detectors" of edge currents. The front gates (F) are used to bring the opposite edge currents (indicated by arrows) close to each other to form two tunneling junctions. Applying voltage to the central gate creates an antidot in the middle and controls the number n of quasiholes contained there. An additional side gate (G) can be used to change the shape and the length of one of the paths in the interferometer.

Indeed, a setup that is rather similar to the Mach-Zehnder interferometer described in Section 3 has been experimentally realized in a quantum Hall system [87]. This interferometer has, so far, only achieved functionality in the integer quantum Hall regime (though, even there, the physical observations are not completely understood [88,89]), but it should be able, in principle, to detect the presence of braiding statistics [90,91,92], and even discern whether a system possesses non-Abelian statistics [93]. Unfortunately however, there is a crucial and debilitating difference between the FQH Mach-Zehnder interferometer of [87] and the Mach-Zehnder interferometer described in Section 3: because of the chiral nature of FQH edge currents, one of the detectors and its drain are unavoidably situated *inside* the central interferometry region. As a result, probe anyons accumulate in this region, effectively altering the target anyon's charge. This effect renders the interferometer incapable of measuring a target charge, and hence, useless for qubit readout in topological quantum computation.

Fortunately, there is another type of interferometer that can be constructed in quantum Hall systems which *is* capable of measuring a target charge: the double point-contact interferometer. Moreover, such interferometers, which are of the Fabry–Pérot type [94], involving higher orders of interference, have already achieved experimental functionality in the fractional quantum Hall regime [22]. The double point-contact interferometer was first proposed for use in FQH systems in Ref. [95], where it was analyzed for the Abelian states. It was analyzed for the Moore–Read state [31], the most likely physical realization of non-Abelian statistics, expected to occur at $\nu = 5/2$ and $7/2$ filling fractions, in Refs. [96,69,97,98].

See also [99,100,101,102,103,104,**?**] for related matters. It was further analyzed for arbitrary anyon models, and specifically for all the Read–Rezayi states [36], in particular, the one expected to occur at $\nu = 12/5$ filling fraction, in Ref. [85] (and subsequently analyzed for the $\nu = 12/5$ Read–Rezayi state with homoplastic techniques in Refs. [105,106]). In all of these previous analyses for non-Abelian states, the results were given to lowest order in the tunneling amplitude, and only for target anyons that were assumed to be in a state of definite anyonic charge (i.e. already collapsed). In what follows, we provide expressions including all orders of tunneling, both to explicitly display the unitarity of the quantum evolution and to account for potentially measureable corrections. Furthermore, we allow the target to be in a superposition of different anyonic charges, and relate the results to the analysis of Section 3, so that we now have a proper description of the measurement collapse behavior for these interferometers. Experimental efforts in realization of the double point-contact interferometer have been carried out for Abelian FQH states [22,23,24,25,26,27]. Whether or not these experiments have conclusively demonstrated fractional statistics of excitations in the Abelian FQHE regime remains a topic of some debate [107,108] [4] .

The double point-contact interferometer consists of a quantum Hall bar with two constrictions (point-contacts) and (at least) two antidots, A_1 and A_2, in between them, as depicted in Fig. 3. The constrictions are created by applying voltage to the front gates (F) on top of the Hall bar; by adjusting this voltage, one may control the tunneling amplitudes t_1 and t_2. In the absence of inter-edge tunneling, the gapped bulk of the FQH liquid gives rise to a quantized Hall conductance: $G_{xy} = I/\left(V_{D_\leftarrow} - V_{S_\rightarrow}\right) = \nu e^2/h$, where the current through the Hall bar is $I = \left(I_{D_\leftarrow} - I_{S_\rightarrow}\right)$. At the same time, the diagonal resistance vanishes: $R_{xx} = \left(V_{D_\leftarrow} - V_{S_\leftarrow}\right)/I = 0$. Tunneling current between the opposite edges leads to a deviation of G_{xy} from its quantized value, or equivalently, to the appearance of $G_{xx} \propto R_{xx} \neq 0$. By measuring the diagonal conductance G_{xx}, one effectively measures the interference between the two tunneling paths around the antidot. The tunneling amplitudes t_1 and t_2 must be kept small, to ensure that the tunneling current is completely due to quasiholes rather than composite excitations. Treating tunneling as a perturbation, one can use renormalization group (RG) methods to compare various contributions to the overall current. Such analysis shows that in the weak tunneling regime, the tunneling current at a single point-contact has the dependence $I \propto V^{4s-1}$ where s is the scaling dimension/spin of the corresponding fields/anyons [28,101,102]. It follows that the dominant contribution in this regime is from the field with lowest scaling dimension, which, in FQH systems, is

[4] One of the reasons for the uncertainty in interpreting the results of the experiments testing the Abelian statistics in the FQH regime is the fact that the statistical angle and the conventional Aharonov–Bohm phase acquired by a charged quasiparticle in a magnetic field are not easy to tell apart (this point is discussed in Refs. [109,95]). From this perspective, a non-Abelian FQH state might have an advantage, being that its effect from braiding statistics dramatically differs from the charge-background field contribution.

the fundamental quasihole. It should be noted that the quasihole tunneling is actually relevant in the RG sense, which, in more physical terms, translates into the tendency of these point contacts to become effectively pinched off in the limit of zero temperature and zero bias. On a more mundane level, the quantum Hall liquid can be broken into separate puddles by the introduction of a constriction due to purely electrostatic effects (such as edges not being sufficiently sharp). In this regard, the recent experimental evidence [110], indicating that it is possible to construct a point-contact for which the $\nu = 5/2$ state persists in the tunneling region, is reassuring.

The two antidots are used to store two clusters of non-Abelian quasiparticles, A_1 and A_2 respectively, whose combined anyonic charge is being probed. The reason for two antidots, rather than just one (as has been previously suggested in [95,96,97,98,85]), is to allow for the combined target to maintain a coherent superposition of anyonic charges without decoherence from energetics that become important at short range. In particular, the energy splitting between the states of different anyonic charge on an antidot is expected to scale as L^{-1} (where L is the linear size of the dot) due to both kinetic (different angular momentum) and potential (different Coulomb energy) effects [98]. On the other hand, for two separated antidots, this energy difference should vanish exponentially with the distance between them, with suppression determined by the gap [69].

In order to appropriately examine the resulting interference patterns, we envision several experimentally variable parameters: (i) the central gate voltages allowing one to control the number of quasiholes on the antidots, (ii) the perpendicular magnetic field, (iii) the back gate voltage controlling the uniform electron density, and (iv) a side gate (G) that can be used to modify the shape of the edge (and, hence, total area and background flux within) the central interferometry region. The reason for proposing all these different controls is to be able to separately vary the Abelian Aharonov-Bohm phase and the number of quasiholes on the antidots. In fact, having all these different controls may turn out to be redundant, but they may prove beneficial for experimental success.

The target anyon A, is the combination of the anyons A_1, A_2, and all others (including strays) situated inside the central interferometry region. In general, any edge excitation qualifies as a probe anyon, but since tunneling is dominated by the fundamental quasiholes, we can effectively allow the probes to have definite anyonic charge b equal to that of the fundamental quasihole. Letting $(1, 0)$ and $(0, 1)$ correspond to the top and bottom edge, respectively (also denoted as $s = \leftarrow, \rightarrow$, respectively), the unitary evolution operator for a probe anyon B entering the system along the edge is given by

$$U = \begin{bmatrix} r_1^* r_2^* e^{i\theta_{\rm I}} R_{AB} W_{AB} R_{CB} & \frac{1}{t_1^*}\left(1 - |r_1|^2 W_{BA}\right) \\ R_{BC}\frac{1}{t_2}\left(-1 + |r_2|^2 W_{AB}\right) R_{CB} & r_1 r_2 e^{i\theta_{\rm II}} R_{BC} R_{BA} W_{BA} \end{bmatrix}, \tag{4.1}$$

when the C anyons (those outside the central interferometry region that are entangled with A) are in the region to the right of central, where we have defined

$$\begin{aligned} W_{AB} &= \sum_{n=0}^{\infty} \left(-t_1^* t_2 e^{i(\theta_{\rm I}+\theta_{\rm II})} R_{BA} R_{AB}\right)^n \\ &= \left[1 + t_1^* t_2 e^{i(\theta_{\rm I}+\theta_{\rm II})} R_{BA} R_{AB}\right]^{-1}. \end{aligned} \tag{4.2}$$

The phases $\theta_{\rm I}$ and $\theta_{\rm II}$ are respectively picked up from traveling counter-clockwise along the top and bottom edge around the central interferometry region, and include the contribution from the enclosed background magnetic field. We note that when higher order terms are significant, it might be the case that tunneling contributions from excitations other than the fundamental quasiholes (which have different tunneling amplitudes) are also important, but nevertheless proceed with considering all orders of tunneling in this manner. The tunneling matrices are

$$T_j = \begin{bmatrix} r_j^* & t_j \\ -t_j^* & r_j \end{bmatrix} \tag{4.3}$$

with $j = 1, 2$ for the left and right point contacts, respectively. We can perform a similar density matrix calculation as for the Mach-Zehnder interferometer, except with more complicated diagrams in this case. Sending a single probe particle in from the bottom edge ($s = \rightarrow$) (which is effectively done by applying a bias voltage across the edges), and detecting it coming out at the bottom or top edge gives the same form for the resulting density matrix as in Eq. (3.28), except with more complicated $p^s_{aa'e,b}$ that are determined by using U of Eq. (4.1) for VU in Eqs. (3.9–3.11). To order $|t|^2$ (for $|t_1| \sim |t_2|$ small), we find

$$\begin{aligned} p^{\rightarrow}_{aa'e,b} &\simeq |r_1|^2 |r_2|^2 \left(1 - t_1^* t_2 e^{i(\theta_{\rm I}+\theta_{\rm II})} M_{ab} - t_1 t_2^* e^{-i(\theta_{\rm I}+\theta_{\rm II})} M^*_{a'b}\right) \\ &\simeq 1 - |t_1|^2 - |t_2|^2 - |t_1 t_2| \left(e^{i\beta} M_{ab} + e^{-i\beta} M^*_{a'b}\right) \end{aligned} \tag{4.4}$$

and

$$\begin{aligned} p^{\leftarrow}_{aa'e,b} &\simeq |t_1|^2 + |r_1|^2 t_1^* t_2 e^{i(\theta_{\rm I}+\theta_{\rm II})} M_{ab} \\ &\quad + |r_1|^2 t_1 t_2^* e^{-i(\theta_{\rm I}+\theta_{\rm II})} M^*_{a'b} + |r_1|^4 |t_2|^2 M_{eb} \\ &\simeq |t_1|^2 + |t_1 t_2| \left(e^{i\beta} M_{ab} + e^{-i\beta} M^*_{a'b}\right) + |t_2|^2 M_{eb} \end{aligned} \tag{4.5}$$

where we have defined $\beta = \arg\left\{t_1^* t_2 e^{i(\theta_{\rm I}+\theta_{\rm II})}\right\}$. We see that

$$p^{\rightarrow}_{aa'e,b} + p^{\leftarrow}_{aa'e,b} \simeq |t_2|^2 M_{eb} + |r_2|^2 . \tag{4.6}$$

Here we have $|t_2|^2$ as the probability of the probe B passing between anyons A and C, rather than $|t_1|^2$, as in the case analyzed for the Mach-Zehnder interferometer, because of the location of C. The values for the two outcome probabilities (i.e. the $e = 1$ terms) to all orders are

$$\begin{aligned}
p^{\rightarrow}_{aa1,b} &= \sum_c N^c_{ab} \frac{d_c}{d_a d_b} \frac{|r_1|^2 |r_2|^2}{\left|1 + t_1^* t_2 e^{i(\theta_{\rm I}+\theta_{\rm II})} e^{i2\pi(s_c - s_a - s_b)}\right|^2} \\
&= \sum_c N^c_{ab} \frac{d_c}{d_a d_b} \frac{|r_1|^2 |r_2|^2}{1 + |t_1|^2 |t_2|^2 + 2|t_1 t_2| \cos\left[\beta + 2\pi(s_c - s_a - s_b)\right]} \qquad (4.7) \\
&\simeq 1 - |t_1|^2 - |t_2|^2 - 2|t_1 t_2| \,\mathrm{Re}\left\{e^{i\beta} M_{ab}\right\} \qquad (4.8) \\
p^{\leftarrow}_{aa1,b} &= 1 - p^{\rightarrow}_{aa1,b}. \qquad (4.9)
\end{aligned}$$

These are also the values of $p^s_{aa'e,b}$ to all orders when $M_{eb} = 1$, but in general $p^s_{aa'e,b}$ does not have such a nice form. One may also perform edge current tunneling calculations employing the conformal field theoretic description of the edge modes in order to determine the effects of the source-drain voltage, the separation length between the two point-contacts, and the temperature [95] (see also [28,101,102,103,106]). The result of such considerations is essentially an interference suppressing Q-factor [recall the discussion following Eq. (3.20)] that decreases (with modulation) as any of these three quantities increase. There may be additional sources of interference suppression, such as switching noise [99] or edge-bulk tunneling [104,**?**]. Though the suppression factor is only close to $Q = 1$ in certain regimes, we will again ignore it, but keep its existence in the back of our minds.

As before, the target system collapses onto states with common values of $p^{\rightarrow}_{aa1,b}$, generically producing a density matrix with non-zero elements that correspond to difference charges e with $M_{eb} = 1$ (and $M_{ab} = M_{a'b}$). To first order, the behavior is essentially identical to that of the Mach-Zehnder interferometer which we previously obtained, but the higher order terms may require more stringent conditions for superpositions to survive measurement collapse than just indistinguishability of monodromy scalar components (since this only guarantees proper matching to first order). Specifically, for superpositions of a and a' to survive, they must have

$$\sum_c N^c_{ab} \frac{d_c}{d_a} \left(\frac{\theta_c}{\theta_a}\right)^n = \sum_c N^c_{a'b} \frac{d_c}{d_{a'}} \left(\frac{\theta_c}{\theta_{a'}}\right)^n \tag{4.10}$$

for all n, and some much more cumbersome condition for the survival of coherent superpositions corresponding to difference charge e. However, it seems that this condition is often equivalent to indistinguishability of monodromy scalar components for models of interest. In order to have $p^{\leftarrow}_{aa1,b} = 0$, i.e. producing sometimes

perfect distinguishability[5], we require equal tunneling probabilities $|t_1| = |t_2|$, and $\cos[\beta + 2\pi(s_c - s_a - s_b)] = -1$ for all $N_{ab}^c \neq 0$. In Eq. (3.80), we obtained an estimate for the total number of probes, $N \gtrsim \left(\frac{z^*_{\alpha/2}}{t\Delta M}\right)^2$, needed to collapse and distinguish a superposition of two anyonic charges in the target, with some level of confidence $1-\alpha$. Translating this into the amount of time τ necessary for such a measurement, we get the estimate $\tau \gtrsim \frac{e}{|I_{\text{tot}}|}\left(\frac{z^*_{\alpha/2}}{t\Delta M}\right)^2$, where I_{tot} is the total edge current.

From these results, we find that when the target is in a state of definite charge a (or, more generally, in a fixed state ρ_κ with $a \in \mathcal{C}_\kappa$), the longitudinal conductance will be proportional to the probability of the probe injected along the bottom edge to be "detected" exiting along the top edge:

$$G_{xx} \propto p^{\leftarrow}_{aa1,b} \simeq |t_1|^2 + |t_2|^2 + 2|t_1 t_2| \,\text{Re}\left\{e^{i\beta} M_{ab}\right\} \tag{4.11}$$

which is exactly Eq. (7) in Ref. [85]. This is an experimentally measurable quantity, found by measuring the voltage between $S_\rightarrow$ and $D_\leftarrow$. Using the side gate (G), one can vary β and, from the resulting modulation in the conductance, determine the amplitude of M_{ab}. Indeed, the measurement of this quantity may be used to help properly identify the topological order of an unknown physical state.

4.1 Predictions for FQH States

The results of this section are applicable to any FQH state. Because of their relative significance, we will only give the explicit details here for the Abelian hierarchy states, the Moore–Read state, and the (particle-hole conjugate of the) $k = 3, M = 1$ Read–Rezayi state. The anyon models of these FQH states may be easily described in terms of those given in Section 3.6. The application of this section's results to the entire Read–Rezayi series and the NASS states of [44] may be found in [79] (and partially in [85]). In all these FQH examples, it is important to remember that the electric charge and anyonic charge are coupled through Abelian terms for FQH states. Consequently, superselection of electric charge only permits superposition of anyonic charges that correspond to the same electric charge (i.e. are composed of the same number of fundamental quasiholes).

4.1.1 The Abelian Hierarchy States ($\nu = n/m$)

The Abelian fractional quantum Hall states can all be constructed from $\mathbb{Z}_N$ models. The general formulation in terms of K matrices may be found in [111], but we will

[5] One can never have *always* perfect distinguishability for this interferometer, since it must be in the weak tunneling limit, which prevents ever having $|t_j|^2 = 1/2$.

describe the Laughlin and hierarchy states [112,113,114,115] that occur at filling fractions $\nu = n/m$ (with m odd and $n < m$). As shown in [31], the statistical factor of the fundamental quasihole in these states is $\theta = \frac{\pi p}{m}$ where p is odd and $np \equiv 1 \bmod m$ (which uniquely defines p modulo $2m$). It follows that these states are described by $\mathbb{Z}_{2m}^{(p)}$ of Section 3.6.1, in which a fundamental quasihole has anyonic charge $[1]_{2m}$ and electric charge e/m, while an electron (which has electric charge $-e$) has anyonic charge $[m]_{2m}$. Using $b = [1]_{2m}$ probes, we have

$$p^{\leftarrow}_{aa0,b} = 1 - \frac{|r_1|^2 |r_2|^2}{\left|1 + |t_1 t_2|\, e^{i\left(\beta + n\frac{2\pi p}{m}\right)}\right|^2} \tag{4.12}$$

$$\simeq |t_1|^2 + |t_2|^2 + 2|t_1 t_2| \cos\left(\beta + n\frac{2\pi p}{m}\right), \tag{4.13}$$

and all permissible states are automatically fixed states with the target system's anyons A and C having definite charge

$$\rho_a^A = |a, c; [a+c]_{2m}\rangle \langle a, c; [a+c]_{2m}| \,. \tag{4.14}$$

4.1.2 The Moore–Read State ($\nu = 5/2, 7/2$)

The anyon model corresponding to the Moore–Read state, expected to describe the $\nu = 5/2, 7/2$ plateaus, is given by [79]:

$$\begin{aligned} \text{MR} &= \text{Ising} \times \mathbb{Z}_8^{(1/2)}\Big|_{\mathcal{C}} \\ \mathcal{C} &= \{(1, [2m]_8), (\sigma, [2m+1]_8), (\psi, [2m]_8)\} \end{aligned} \tag{4.15}$$

(for $m \in \mathbb{Z}$), the restriction of the direct product of the Ising and $\mathbb{Z}_8^{(1/2)}$ anyon models to the charge spectrum $\mathcal{C} \subset \mathcal{C}_{\text{Ising}} \times \mathcal{C}_{\mathbb{Z}_8^{(1/2)}}$ in which the 1 and ψ Ising charges are paired with the even sector of $\mathbb{Z}_8^{(1/2)}$ and the σ Ising charge is paired with the odd sector of $\mathbb{Z}_8^{(1/2)}$. Writing $a = (a_{\text{I}}, a_{\mathbb{Z}}) \in \mathcal{C}$, where $a_{\text{I}} \in \mathcal{C}_{\text{Ising}}$ and $a_{\mathbb{Z}} \in \mathcal{C}_{\mathbb{Z}_8^{(1/2)}}$, this is more explicitly given by

$\mathcal{C} = \{(1, [2m]_8), (\sigma, [2m+1]_8), (\psi, [2m]_8)\}, \quad N_{ab}^c = N_{a_{\text{I}} b_{\text{I}}}^{c_{\text{I}}} N_{a_{\mathbb{Z}} b_{\mathbb{Z}}}^{c_{\mathbb{Z}}}$		
$\left[F_d^{abc}\right]_{ef} = \left[F_{d_{\text{I}}}^{a_{\text{I}} b_{\text{I}} c_{\text{I}}}\right]_{e_{\text{I}} f_{\text{I}}} \left[F_{d_{\mathbb{Z}}}^{a_{\mathbb{Z}} b_{\mathbb{Z}} c_{\mathbb{Z}}}\right]_{e_{\mathbb{Z}} f_{\mathbb{Z}}}, \quad \left[F_{cd}^{ab}\right]_{ef} = \left[F_{c_{\text{I}} d_{\text{I}}}^{a_{\text{I}} b_{\text{I}}}\right]_{e_{\text{I}} f_{\text{I}}} \left[F_{c_{\mathbb{Z}} d_{\mathbb{Z}}}^{a_{\mathbb{Z}} b_{\mathbb{Z}}}\right]_{e_{\mathbb{Z}} f_{\mathbb{Z}}}$		
$R_c^{ab} = R_{c_{\text{I}}}^{a_{\text{I}} b_{\text{I}}} R_{c_{\mathbb{Z}}}^{a_{\mathbb{Z}} b_{\mathbb{Z}}}$	$S_{ab} = \sqrt{2} S_{a_{\text{I}} b_{\text{I}}} S_{a_{\mathbb{Z}} b_{\mathbb{Z}}}$	$M_{ab} = M_{a_{\text{I}} b_{\text{I}}} M_{a_{\mathbb{Z}} b_{\mathbb{Z}}}$
$d_a = d_{a_{\text{I}}}, \quad \mathcal{D} = 4$		$\theta_a = \theta_{a_{\text{I}}} \theta_{a_{\mathbb{Z}}}$

where all the symbols (N, F, R, S, M, d, θ) labeled by subscript I charges are those of the Ising model given in the table of Section 3.6.3, and those with subscript $\mathbb{Z}$

charges are those of the $\mathbb{Z}_8^{(1/2)}$ anyon model given in the table of Section 3.6.1. The factor of $\sqrt{2}$ arises in front of the product of S-matrices because of the restriction of the charge spectrum. The fundamental quasihole has anyonic charge $(\sigma, [1]_8)$ and electric charge $e/4$. The electron has anyonic charge $(\psi, [4]_8)$.

The target system's anyons A and C may by thought of as composed of n and m fundamental quasiholes, respectively (with electric charges $ne/4$ and $me/4$), where n, m are integers (possibly negative). If n is even, the target's total anyonic charge may be in some superposition of $(1, [n]_8)$ and $(\psi, [n]_8)$. If n is odd, the target anyon has total anyonic charge $(\sigma, [n]_8)$. The same holds for the target's entangled partner C. We will employ the shorthand $x_n = (x, [n]_8)$, with $x = 1, \sigma, \psi$. For probe anyons that are fundamental quasiholes, $b = \sigma_1$, this gives

$$p^{\leftarrow}_{1_n 1_n 1_0, \sigma_1} = 1 - \frac{|r_1|^2 |r_2|^2}{\left|1 + |t_1 t_2| \, e^{i\left(\beta + n\frac{\pi}{4}\right)}\right|^2} \tag{4.16}$$

$$\simeq |t_1|^2 + |t_2|^2 + 2|t_1 t_2| \cos\left(\beta + n\frac{\pi}{4}\right) \tag{4.17}$$

$$p^{\leftarrow}_{\psi_n \psi_n 1_0, \sigma_1} = 1 - \frac{|r_1|^2 |r_2|^2}{\left|1 - |t_1 t_2| \, e^{i\left(\beta + n\frac{\pi}{4}\right)}\right|^2} \tag{4.18}$$

$$\simeq |t_1|^2 + |t_2|^2 - 2|t_1 t_2| \cos\left(\beta + n\frac{\pi}{4}\right) \tag{4.19}$$

$$p^{\leftarrow}_{\sigma_n \sigma_n 1_0, \sigma_1} = 1 - \frac{|r_1|^2 |r_2|^2 \left(1 + |t_1 t_2|^2\right)}{\left|1 - (-1)^{\frac{n-1}{2}} |t_1 t_2|^2 \, e^{i2\beta}\right|^2} \tag{4.20}$$

$$\simeq |t_1|^2 + |t_2|^2 - 2|t_1 t_2|^2 \left[1 + (-1)^{\frac{n-1}{2}} \cos(2\beta)\right]. \tag{4.21}$$

With these probes (and electric charge superselection), all charges are distinguishable, so the charge classes $\mathcal{C}_\kappa$ are all singletons and interferometry will collapse any superposition of charge in the target onto a definite charge state. Of specific note is that for n odd, the interference is suppressed. The leading order modulation occurs at fourth order in t, and has the twice the modulation frequency. In fact, higher order harmonics enter as modulations in $2j\beta$ that are $4j^{th}$ order in t. When m is even, the probabilities and fixed states are

$$\Pr_A(\kappa_{1_n}) = \rho_{(1_n, 1_m; 1_{n+m})(1_n, 1_m; 1_{n+m})} + \rho_{(1_n, \psi_m; \psi_{n+m})(1_n, \psi_m; \psi_{n+m})} \tag{4.22}$$

$$\rho^A_{\kappa_{1_n}} = \frac{1}{\Pr_A(\kappa_{1_n})} \Big\{ \rho_{(1_n, 1_m; 1_{n+m})(1_n, 1_m; 1_{n+m})} \, |1_n, 1_m; 1_{n+m}\rangle \langle 1_n, 1_m; 1_{n+m}| + \rho_{(1_n, \psi_m; \psi_{n+m})(1_n, \psi_m; \psi_{n+m})} \, |1_n, \psi_m; \psi_{n+m}\rangle \langle 1_n, \psi_m; \psi_{n+m}| \Big\} \tag{4.23}$$

$$\Pr_A(\kappa_{\sigma_n}) = \rho_{(\sigma_n,1_m;\sigma_{n+m})(\sigma_n,1_m;\sigma_{n+m})} + \rho_{(\sigma_n,\psi_m;\sigma_{n+m})(\sigma_n,\psi_m;\sigma_{n+m})} \tag{4.24}$$

$$\begin{aligned}\rho^A_{\kappa_{\sigma_n}} = &\frac{1}{\Pr_A(\kappa_{\sigma_n})}\frac{1}{\sqrt{2}} \\ &\times\Big\{\rho_{(\sigma_n,1_m;\sigma_{n+m})(\sigma_n,1_m;\sigma_{n+m})}\left|\sigma_n,1_m;\sigma_{n+m}\right\rangle\left\langle\sigma_n,1_m;\sigma_{n+m}\right| \\ &\quad+\rho_{(\sigma_n,\psi_m;\sigma_{n+m})(\sigma_n,\psi_m;\sigma_{n+m})}\left|\sigma_n,\psi_m;\sigma_{n+m}\right\rangle\left\langle\sigma_n,\psi_m;\sigma_{n+m}\right|\Big\}\end{aligned} \tag{4.25}$$

$$\Pr_A(\kappa_{\psi_n}) = \rho_{(\psi_n,1_m;\psi_{n+m})(\psi_n,1_m;\psi_{n+m})} + \rho_{(\psi_n,\psi_m;1_{n+m})(\psi_n,\psi_m;1_{n+m})} \tag{4.26}$$

$$\begin{aligned}\rho^A_{\kappa_{\psi_n}} = &\frac{1}{\Pr_A(\kappa_{\psi_n})}\Big\{\rho_{(\psi_n,1_m;\psi_{n+m})(\psi_n,1_m;\psi_{n+m})}\left|\psi_n,1_m;\psi_{n+m}\right\rangle\left\langle\psi_n,1_m;\psi_{n+m}\right| \\ &\quad+\rho_{(\psi_n,\psi_m;1_{n+m})(\psi_n,\psi_m;1_{n+m})}\left|\psi_n,\psi_m;1_{n+m}\right\rangle\left\langle\psi_n,\psi_m;1_{n+m}\right|\Big\}\end{aligned} \tag{4.27}$$

and when m is odd, they are

$$\Pr_A(\kappa_{1_n}) = \rho_{(1_n,\sigma_m;\sigma_{n+m})(1_n,\sigma_m;\sigma_{n+m})} \tag{4.28}$$

$$\rho^A_{\kappa_{1_n}} = \frac{1}{\sqrt{2}}\left|1_n,\sigma_m;\sigma_{n+m}\right\rangle\left\langle1_n,\sigma_m;\sigma_{n+m}\right| \tag{4.29}$$

$$\Pr_A(\kappa_{\sigma_n}) = \rho_{(\sigma_n,\sigma_m;1_{n+m})(\sigma_n,\sigma_m;1_{n+m})} + \rho_{(\sigma_n,\sigma_m;\psi_{n+m})(\sigma_n,\sigma_m;\psi_{n+m})} \tag{4.30}$$

$$\rho^A_{\kappa_{\sigma_n}} = \frac{1}{2}\left[\left|\sigma_n,\sigma_m;1_{n+m}\right\rangle\left\langle\sigma_n,\sigma_m;1_{n+m}\right| + \left|\sigma_n,\sigma_m;\psi_{n+m}\right\rangle\left\langle\sigma_n,\sigma_m;\psi_{n+m}\right|\right] \tag{4.31}$$

$$\Pr_A(\kappa_{\psi_n}) = \rho_{(\psi_n,\sigma_m;\sigma_{n+m})(\psi_n,\sigma_m;\sigma_{n+m})} \tag{4.32}$$

$$\rho^A_{\kappa_{\psi_n}} = \frac{1}{\sqrt{2}}\left|\psi_n,\sigma_m;\sigma_{n+m}\right\rangle\left\langle\psi_n,\sigma_m;\sigma_{n+m}\right| \tag{4.33}$$

If one had a way to effectively suppress the tunneling of fundamental quasiholes, then the next most dominant contribution to tunneling comes from excitations with anyonic charge $b = (1, [2]_8)$, which are Abelian, and give (with different values of T_j)

$$p^{\leftarrow}_{x_n x_n 1_0,1_2} = 1 - \frac{|r_1|^2\,|r_2|^2}{\left|1 + |t_1 t_2|\, e^{i\left(\beta + n\frac{\pi}{2}\right)}\right|^2} \tag{4.34}$$

$$\simeq |t_1|^2 + |t_2|^2 + 2\,|t_1 t_2|\cos\left(\beta + n\frac{\pi}{2}\right). \tag{4.35}$$

The Ising charges are obviously indistinguishable when the probe has Ising charge 1, so superpositions of 1 and ψ will not be affected by these probes (i.e. all allowed target density matrices are fixed states). If we had sufficiently good precision and control over the experimental variables to set them exactly to $|t_1| = |t_2| = t$

and $\cos\left(\beta + n\frac{\pi}{4}\right) = -1$ for $a = (1, [n]_8)$ and $b = (\sigma, [1]_8)$, then we would find $p^{\leftarrow}_{aa1,b} = 0$ to all orders, providing a method of suppressing tunneling of fundamental quasiholes. (These settings would give $p^{\leftarrow}_{aa1,b} = \frac{4t^2}{(1+t^2)^2}$ for $a = (\psi, [n]_8)$.) Using this value of β for $b = (1, [2]_8)$ probes gives

$$p^{\leftarrow}_{1_n 1_n 1_0, 1_2} = 1 - \frac{(1-t^2)^2}{\left|1 - t^2 e^{in\frac{\pi}{4}}\right|^2} \tag{4.36}$$

$$\simeq 2t^2 \left[1 - \cos\left(n\pi/4\right)\right]. \tag{4.37}$$

Again, tunneling of these probes will be suppressed when $n \equiv 0 \bmod 8$, and the next most dominant tunneling contribution will be from $b = (\psi, [2]_8)$, giving $p^{\leftarrow}_{1_n 1_n 1_0, \psi_2} = 4t^2$.

4.1.3 The Read–Rezayi State ($\nu = 12/5$)

The anyon model corresponding to the state expected to describe the $\nu = 12/5$ plateau is [79]:

$$\overline{\text{RR}}_{3,1} = \overline{\text{Fib}} \times \mathbb{Z}_{10}^{(3)}, \tag{4.38}$$

the particle-hole conjugate of the $k = 3, M = 1$ Read–Rezayi state [6]. Writing $a = (a_{\text{F}}, a_{\mathbb{Z}}) \in \mathcal{C}$, where $a_{\text{F}} \in \mathcal{C}_{\overline{\text{Fib}}}$ and $a_{\mathbb{Z}} \in \mathcal{C}_{\mathbb{Z}_{10}^{(3)}}$, this is more explicitly given by

$\mathcal{C} = \{(1, [n]_{10}), (\varepsilon, [n]_{10})\}, \quad N_{ab}^{c} = N_{a_{\text{F}} b_{\text{F}}}^{c_{\text{F}}} N_{a_{\mathbb{Z}} b_{\mathbb{Z}}}^{c_{\mathbb{Z}}}$		
$\left[F_d^{abc}\right]_{ef} = \left[F_{d_{\text{F}}}^{a_{\text{F}} b_{\text{F}} c_{\text{F}}}\right]_{e_{\text{F}} f_{\text{F}}} \left[F_{d_{\mathbb{Z}}}^{a_{\mathbb{Z}} b_{\mathbb{Z}} c_{\mathbb{Z}}}\right]_{e_{\mathbb{Z}} f_{\mathbb{Z}}}, \quad \left[F_{cd}^{ab}\right]_{ef} = \left[F_{c_{\text{F}} d_{\text{F}}}^{a_{\text{F}} b_{\text{F}}}\right]_{e_{\text{F}} f_{\text{F}}} \left[F_{c_{\mathbb{Z}} d_{\mathbb{Z}}}^{a_{\mathbb{Z}} b_{\mathbb{Z}}}\right]_{e_{\mathbb{Z}} f_{\mathbb{Z}}}$		
$R_c^{ab} = R_{c_{\text{F}}}^{a_{\text{F}} b_{\text{F}}} R_{c_{\mathbb{Z}}}^{a_{\mathbb{Z}} b_{\mathbb{Z}}}$	$S_{ab} = S_{a_{\text{F}} b_{\text{F}}} S_{a_{\mathbb{Z}} b_{\mathbb{Z}}}$	$M_{ab} = M_{a_{\text{F}} b_{\text{F}}} M_{a_{\mathbb{Z}} b_{\mathbb{Z}}}$
$d_a = d_{a_{\text{F}}}, \quad \mathcal{D} = \sqrt{10\left(\phi + 2\right)}$		$\theta_a = \theta_{a_{\text{F}}} \theta_{a_{\mathbb{Z}}}$

where $n \in \mathbb{Z}$, and all the symbols $(N, F, R, S, M, d, \theta)$ labeled by subscript F charges are those of the $\overline{\text{Fib}}$ given as the complex conjugate of those in the table of Section 3.6.2, and those with subscript $\mathbb{Z}$ charges are those of the $\mathbb{Z}_{10}^{(3)}$ anyon model given in the table of Section 3.6.1. The fundamental quasihole has anyonic charge $(\varepsilon, [1]_{10})$ and electric charge $e/5$. The electron has anyonic charge $(1, [5]_{10})$. Being a direct product of $\overline{\text{Fib}}$ and an Abelian theory, universal topological quantum computation could be achieved through braiding quasiholes of this system.

The target system's anyons A and C carrying total electric charges $ne/5$ and $me/5$, respectively, have $a_{\mathbb{Z}} = [n]_{10}$ and $c_{\mathbb{Z}} = [m]_{10}$, and may be in superpositions of

[6] In general, the anyon models describing the k, M odd Read–Rezayi states may be written neatly as the direct product of anyon models $\text{RR}_{k,M} = \text{SO}(3)_k \times \mathbb{Z}_{2(kM+2)}^{((k(kM+2)-M)/2)}$ [79].

$a_{\rm F}, c_{\rm F} = 1, \varepsilon$. We employ the shorthand (similar to before) $x_n = (x, [n]_{10})$, with $x = 1, \varepsilon$. For probe anyons that are fundamental quasiholes, $b = \varepsilon_1$, this gives

$$p^{\leftarrow}_{1_n 1_n 1_0, \varepsilon_1} \simeq |t_1|^2 + |t_2|^2 + 2\,|t_1 t_2| \cos\left(\beta - n\frac{4\pi}{5}\right) \tag{4.39}$$

$$p^{\leftarrow}_{\varepsilon_n \varepsilon_n 1_0, \varepsilon_1} \simeq |t_1|^2 + |t_2|^2 - 2\phi^{-2}\,|t_1 t_2| \cos\left(\beta - n\frac{4\pi}{5}\right). \tag{4.40}$$

With these probes (and electric charge superselection), all charges are distinguishable, so the charge classes $\mathcal{C}_\kappa$ are all singletons and interferometry will collapse any superposition of charge in the target onto a definite charge state. We note that when the target has $\overline{\rm Fib}$ charge ε, the interference is suppressed, though still second order in t. The probabilities and fixed states are

$$\Pr_A(\kappa_{1_n}) = \rho_{(1_n,1_m;1_{n+m})(1_n,1_m;1_{n+m})} + \rho_{(1_n,\varepsilon_m;\varepsilon_{n+m})(1_n,\varepsilon_m;\varepsilon_{n+m})} \tag{4.41}$$

$$\begin{aligned}\rho_1^A = \frac{1}{\Pr_A(\kappa_{1_n})} \Big\{ & \rho_{(1_n,1_m;1_{n+m})(1_n,1_m;1_{n+m})}\, |1_n, 1_m; 1_{n+m}\rangle \langle 1_n, 1_m; 1_{n+m}| \\ & + \phi^{-1} \rho_{(1_n,\varepsilon_m;\varepsilon_{n+m})(1_n,\varepsilon_m;\varepsilon_{n+m})}\, |1_n, \varepsilon_m; \varepsilon_{n+m}\rangle \langle 1_n, \varepsilon_m; \varepsilon_{n+m}| \Big\}\end{aligned} \tag{4.42}$$

$$\begin{aligned}\Pr_A(\kappa_{\varepsilon_n}) = & \rho_{(\varepsilon_n,1_m;\varepsilon_{n+m})(\varepsilon_n,1_m;\varepsilon_{n+m})} \\ & + \rho_{(\varepsilon_n,\varepsilon_m;1_{n+m})(\varepsilon_n,\varepsilon_m;1_{n+m})} + \rho_{(\varepsilon_n,\varepsilon_m;\varepsilon_{n+m})(\varepsilon_n,\varepsilon_m;\varepsilon_{n+m})}\end{aligned} \tag{4.43}$$

$$\begin{aligned}\rho^A_{\kappa_{\varepsilon_n}} = & \frac{1}{\Pr_A(\kappa_{\varepsilon_n})} \Big\{ \phi^{-1} \rho_{(\varepsilon_n,1_m;\varepsilon_{n+m})(\varepsilon_n,1_m;\varepsilon_{n+m})}\, |\varepsilon_n, 1_m; \varepsilon_{n+m}\rangle \langle \varepsilon_n, 1_m; \varepsilon_{n+m}| \\ & + \phi^{-2} \left(\rho_{(\varepsilon_n,\varepsilon_m;1_{n+m})(\varepsilon_n,\varepsilon_m;1_{n+m})} + \rho_{(\varepsilon_n,\varepsilon_m;\varepsilon_{n+m})(\varepsilon_n,\varepsilon_m;\varepsilon_{n+m})} \right) \\ & \times \left[|\varepsilon_n, \varepsilon_m; 1_{n+m}\rangle \langle \varepsilon_n, \varepsilon_m; 1_{n+m}| + |\varepsilon_n, \varepsilon_m; \varepsilon_{n+m}\rangle \langle \varepsilon_n, \varepsilon_m; \varepsilon_{n+m}| \right] \Big\}\end{aligned} \tag{4.44}$$

By varying β, one can distinguish whether $a_{\rm F}$, the $\overline{\rm Fib}$ charge of a target anyon, is 1 or ε, without needing to know the precise value of the phase involved, because the interference fringe amplitude is suppressed by a factor of $\phi^{-2} \approx .38$ for ε. We emphasize that this provides the $\overline{\rm RR}_{3,1}$ state with a distinct advantage over the Moore-Read state with respect to being able to distinguish the non-Abelian anyonic charges that would be used in these systems as the computational basis states for topological qubits (i.e. 1 and ψ for MR vs. 1 and ε for $\overline{\rm RR}_{3,1}$).

Acknowledgements

We thank L. Bonderson, A. Kitaev, I. Klich, and J. Preskill for illuminating discussions, and acknowledge the hospitality of the IQI, Microsoft Station Q, and the Aspen Center for Physics. This work was supported in part by the NSF under Grant No. PHY-0456720 and the ARO under Grant No. W911NF-05-1-0294.

References

[1] H. S. Green, A generalized method of field quantization, Phys. Rev. 90 (1953) 270–273.

[2] K. Drühl, R. Haag, J. E. Roberts, On parastatistics, Commun. Math. Phys. 18 (1970) 204–226.

[3] J. M. Leinaas, J. Myrheim, On the theory of identical particles, Nuovo Cimento B 37B (1977) 1.

[4] F. Wilczek, Magnetic flux, angular momentum, and statistics, Phys. Rev. Lett. 48 (1982) 1144–1146.

[5] F. Wilczek, Quantum mechanics of fractional-spin particles, Phys. Rev. Lett. 49 (1982) 957–959.

[6] G. A. Goldin, R. Menikoff, D. H. Sharp, Comments on "General Theory for Quantum Statistics in Two Dimensions", Phys. Rev. Lett. 54 (1985) 603.

[7] G. Moore, N. Seiberg, Polynomial equations for rational conformal field theories, Phys. Lett. B 212 (1988) 451–460.

[8] G. Moore, N. Seiberg, Classical and quantum conformal field theory, Commun. Math. Phys. 123 (1989) 177–254.

[9] E. Witten, Quantum field theory and the Jones polynomial, Comm. Math. Phys. 121 (1989) 351–399.

[10] K. Fredenhagen, K. H. Rehren, B. Schroer, Superselection sectors with braid group statistics and exchange algebras, Commun. Math. Phys. 125 (1989) 201–226.

[11] J. Fröhlich, F. Gabbiani, Braid statistics in local quantum theory, Rev. Math. Phys. 2 (1990) 251–353.

[12] V. G. Turaev, Quantum Invariants of Knots and 3-Manifolds, Walter de Gruyter, Berlin, New York, 1994.

[13] C. Kassel, Quantum Groups, Springer-Verlag, New York, Berlin, Heidelberg, 1995.

[14] B. Bakalov, A. Kirillov, Lectures on Tensor Categories and Modular Functors, Vol. 21 of University Lecture Series, American Mathematical Society, 2001.

[15] R. Prange, S. M. Girvin (Eds.), The Quantum Hall effect, Springer-Verlag, New York, 1987.

[16] A. Karlhede, S. A. Kivelson, S. L. Sondhi, The quantum Hall effect: The article, in: V. J. Emery (Ed.), Correlated Electron Systems, World Scientific, Singapore, 1992, lectures presented at the 9th Jerusalem Winter School for Theoretical Physics.

[17] S. Das Sarma, A. Pinczek, Perspectives in quantum Hall effects: Novel quantum liquids in low-dimensional semiconductor structures, Wiley, New York, 1997.

[18] Z. Ezawa (Ed.), Quantum Hall effects, field theoretical approach and related topics, World Scientific, Singapore, 2000.

[19] K. von Klitzing, G. Dorda, M. Pepper, New method for high-accuracy determination of the fine-structure constant based on quantized Hall resistance, Phys. Rev. Lett. 45 (1980) 494–497.

[20] D. C. Tsui, H. L. Stormer, A. C. Gossard, Two-dimensional magnetotransport in the extreme quantum limit, Phys. Rev. Lett. 48 (1982) 1559–62.

[21] V. J. Goldman, B. Su, Resonant tunneling in the quantum Hall regime: Measurement of fractional charge, Science 267 (1995) 1010–1012.

[22] V. J. Goldman, J. Liu, A. Zaslavsky, Fractional statistics of Laughlin quasiparticles in quantum antidots, Phys. Rev. B 71 (2005) 153303.

[23] F. E. Camino, W. Zhou, V. J. Goldman, Realization of a Laughlin quasiparticle interferometer: Observation of fractional statistics, Phys. Rev. B 72 (2005) 075342, cond-mat/0502406.

[24] F. E. Camino, W. Zhou, V. J. Goldman, Aharonov–Bohm superperiod in a Laughlin quasiparticle interferometer, Phys. Rev. Lett. 95 (2005) 246802, cond-mat/0504341.

[25] F. E. Camino, W. Zhou, V. J. Goldman, Transport in the Laughlin quasiparticle interferometer: Evidence for topological protection in an anyonic qubit, Phys. Rev. B 74 (2006) 115301, cond-mat/0606742.

[26] F. E. Camino, W. Zhou, V. J. Goldman, $e/3$ Laughlin quasiparticle primary-filling $\nu = 1/3$ interferometer, Phys. Rev. Lett. 98 (2007) 076805, cond-mat/0610751.

[27] F. E. Camino, W. Zhou, V. J. Goldman, Experimental realization of a primary-filling e/3 quasiparticle interferometer (2006), cond-mat/0611443.

[28] X. G. Wen, Theory of the edge states in fractional quantum Hall effects, Intl. J. Mod. Phys. B 6 (1992) 1711–62.

[29] E. V. Tsiper, V. J. Goldman, Formation of an edge striped phase in fractional quantum Hall systems, Phys. Rev. B 64 (2001) 165311, cond-mat/0101151.

[30] X. Wan, K. Yang, E. H. Rezayi, Reconstruction of fractional quantum Hall edges, Phys. Rev. Lett. 88 (2002) 056802, cond-mat/0106386.

[31] G. Moore, N. Read, Nonabelions in the fractional quantum Hall effect, Nucl. Phys. B 360 (1991) 362–396.

[32] R. Willett, J. P. Eisenstein, H. L. Stormer, D. C. Tsui, A. C. Gossard, J. H. English, Observation of an even-denominator quantum number in the fractional quantum Hall effect, Phys. Rev. Lett. 59 (1987) 1776–9.

[33] W. Pan, J.-S. Xia, V. Shvarts, D. E. Adams, H. L. Stormer, D. C. Tsui, L. N. Pfeiffer, K. W. Baldwin, K. W. West, Exact quantization of the even-denominator fractional quantum Hall state at $\nu = 5/2$ Landau level filling factor, Phys. Rev. Lett. 83 (1999) 3530–3, cond-mat/9907356.

[34] J. P. Eisenstein, K. B. Cooper, L. N. Pfeiffer, K. W. West, Insulating and fractional quantum Hall states in the first excited Landau level, Phys. Rev. Lett. 88 (2002) 076801, cond-mat/0110477.

[35] J. S. Xia, W. Pan, C. L. Vicente, E. D. Adams, N. S. Sullivan, H. L. Stormer, D. C. Tsui, L. N. Pfeiffer, K. W. Baldwin, K. W. West, Electron correlation in the second Landau level: A competition between many nearly degenerate quantum phases, Phys. Rev. Lett. 93 (2004) 176809, cond-mat/0406724.

[36] N. Read, E. Rezayi, Beyond paired quantum Hall states: Parafermions and incompressible states in the first excited Landau level, Phys. Rev. B 59 (1999) 8084–8092, cond-mat/9809384.

[37] R. H. Morf, Transition from quantum Hall to compressible states in the second Landau level: new light on the $\nu = 5/2$ enigma, Phys. Rev. Lett. 80 (1998) 1505–8, cond-mat/9809024.

[38] E. H. Rezayi, F. D. M. Haldane, Incompressible paired Hall state, stripe order, and the composite fermion liquid phase in half-filled Landau levels, Phys. Rev. Lett. 84 (2000) 4685–4688, cond-mat/9906137.

[39] C. Nayak, F. Wilczek, $2n$-quasihole states realize 2^{n-1}-dimensional spinor braiding statistics in paired quantum Hall states, Nucl. Phys. B 479 (1996) 529–53, cond-mat/9605145.

[40] J. K. Slingerland, F. A. Bais, Quantum groups and nonabelian braiding in quantum Hall systems, Nucl. Phys. B 612 (2001) 229–290, cond-mat/0104035.

[41] N. Read, D. Green, Paired states of fermions in two dimensions with breaking of parity and time-reversal symmetries and the fractional quantum Hall effect, Phys. Rev. B 61 (2000) 10267–10297, cond-mat/9906453.

[42] D. A. Ivanov, Non-Abelian statistics of half-quantum vortices in p-wave superconductors, Phys. Rev. Lett. 86 (2001) 268–271, cond-mat/0005069.

[43] A. Stern, F. von Oppen, E. Mariani, Geometric phases and quantum entanglement as building blocks for non-Abelian quasiparticle statistics, Phys. Rev. B 70 (2004) 205338, cond-mat/0310273.

[44] E. Ardonne, K. Schoutens, A new class of non-Abelian spin-singlet quantum Hall states, Phys. Rev. Lett. 82 (25) (1999) 5096–5099, cond-mat/9811352.

[45] A. Y. Kitaev, Fault-tolerant quantum computation by anyons, Ann. Phys. 303 (2003) 2, quant-ph/9707021.

[46] A. Kitaev, Anyons in an exactly solved model and beyond, Ann. Phys. 321 (2006) 2–111, cond-mat/0506438.

[47] M. H. Freedman, A magnetic model with a possible Chern-Simons phase, Commun. Math. Phys. 234 (2003) 129–183, quant-ph/0110060.

[48] M. Freedman, C. Nayak, K. Shtengel, K. Walker, Z. Wang, A class of P, T-invariant topological phases of interacting electrons, Ann. Phys. 310 (2004) 428–492, cond-mat/0307511.

[49] M. Freedman, C. Nayak, K. Shtengel, Extended Hubbard model with ring exchange: A route to a non-Abelian topological phase, Phys. Rev. Lett. 94 (2005) 066401, cond-mat/0312273.

[50] M. Freedman, C. Nayak, K. Shtengel, Line of critical points in $2 + 1$ dimensions: Quantum critical loop gases and non-Abelian gauge theory, Phys. Rev. Lett. 94 (2005) 147205, cond-mat/0408257.

[51] V. G. Turaev, O. Y. Viro, State sum invariants of 3-manifolds and quantum 6j-symbols, Topology 31 (1992) 865–902.

[52] M. A. Levin, X.-G. Wen, String-net condensation: A physical mechanism for topological phases, Phys. Rev. B 71 (2005) 045110, cond-mat/0404617.

[53] P. Fendley, E. Fradkin, Realizing non-Abelian statistics in time-reversal-invariant systems, Phys. Rev. B 72 (2005) 024412, cond-mat/0502071.

[54] L. Fidkowski, M. Freedman, C. Nayak, K. Walker, Z. Wang, From string nets to nonabelions (2006), cond-mat/0610583.

[55] B. Douçot, L. B. Ioffe, J. Vidal, Discrete non-Abelian gauge theories in Josephson-junction arrays and quantum computation, Phys. Rev. B 69 (2004) 214501, cond-mat/0302104.

[56] S. Das Sarma, C. Nayak, S. Tewari, Proposal to stabilize and detect half-quantum vortices in strontium ruthenate thin films: Non-Abelian braiding statistics of vortices in a $p_x + ip_y$ superconductor, Phys. Rev. B 73 (2006) 220502, cond-mat/0510553.

[57] S. Tewari, S. Das Sarma, C. Nayak, C. Zhang, P. Zoller, Quantum computation using vortices and Majorana zero modes of a $p_x + ip_y$ superfluid of fermionic cold atoms, Phys. Rev. Lett. 98 (2007) 010506, quant-ph/0606101.

[58] V. Gurarie, L. Radzihovsky, A. V. Andreev, Quantum phase transitions across a p-wave Feshbach resonance, Phys. Rev. Lett. 94 (2005) 230403, cond-mat/0410620.

[59] N. R. Cooper, N. K. Wilkin, J. M. F. Gunn, Quantum phases of vortices in rotating Bose–Einstein condensates, Phys. Rev. Lett. 87 (2001) 120405, cond-mat/0107005.

[60] N. R. Cooper, Exact ground states of rotating Bose gases close to a Feshbach resonance, Physical Review Letters 92 (2004) 220405, cond-mat/0107005.

[61] E. H. Rezayi, N. Read, N. R. Cooper, Incompressible liquid state of rapidly rotating bosons at filling factor 3/2, Phys. Rev. Lett. 95 (2005) 160404, cond-mat/0507064.

[62] J. Preskill, Fault-tolerant quantum computation, in: H.-K. Lo, S. Popescu, T. P. Spiller (Eds.), Introduction to Quantum Computation, World Scientific, 1998, quant-ph/9712048.

[63] R. W. Ogburn, J. Preskill, Topological quantum computation, Lect. Notes in Comp. Sci. 1509 (1999) 341–356.

[64] M. H. Freedman, Quantum computation and the localization of modular functors, Found. Comput. Math. 1 (2001) 183–204, quant-ph/0003128.

[65] M. H. Freedman, M. J. Larsen, Z. Wang, A modular functor which is universal for quantum computation, Commun. Math. Phys. 227 (2002) 605–622, quant-ph/0001108.

[66] M. H. Freedman, A. Kitaev, M. J. Larsen, Z. Wang, Topological quantum computation, Bull. Amer. Math. Soc. (N.S.) 40 (2003) 31–38, quant-ph/0101025.

[67] C. Mochon, Anyons from nonsolvable finite groups are sufficient for universal quantum computation, Phys. Rev. A 67 (2003) 022315, quant-ph/0206128.

[68] C. Mochon, Anyon computers with smaller groups, Phys. Rev. A 69 (2004) 032306, quant-ph/0306063.

[69] S. Das Sarma, M. Freedman, C. Nayak, Topologically protected qubits from a possible non-Abelian fractional quantum Hall state, Phys. Rev. Lett. 94 (2005) 166802, cond-mat/0412343.

[70] M. Freedman, C. Nayak, K. Walker, Towards universal topological quantum computation in the $\nu = 5/2$ fractional quantum Hall state (2005), cond-mat/0512066.

[71] M. Freedman, C. Nayak, K. Walker, Tilted interferometry realizes universal quantum computation in the Ising TQFT without overpasses (2005), cond-mat/0512072.

[72] S. Bravyi, Universal quantum computation with the $\nu = 5/2$ fractional quantum Hall state, Phys. Rev. A 73 (2006) 042313, quant-ph/0511178.

[73] N. E. Bonesteel, L. Hormozi, G. Zikos, S. H. Simon, Braid topologies for quantum computation, Phys. Rev. Lett. 95 (2005) 140503, quant-ph/0505065.

[74] S. H. Simon, N. E. Bonesteel, M. H. Freedman, N. Petrovic, L. Hormozi, Topological quantum computing with only one mobile quasiparticle, Phys. Rev. Lett. 96 (2006) 070503, quant-ph/0509175.

[75] L. Hormozi, G. Zikos, N. E. Bonesteel, S. H. Simon, Topological quantum compiling, Phys. Rev. B 75 (2007) 165310, quant-ph/0610111.

[76] Y. Aharonov, D. Bohm, Significance of electromagnetic potentials in the quantum theory, Phys. Rev. 115 (1959) 485–491.

[77] V. B. Braginsky, Y. I. Vorontsov, Usp. Fiz. Nauk 41–62 (1974) 114, [Sov. Phys. Uspekhi 17, 644 (1975)].

[78] J. Preskill, Topological quantum computation, lecture notes (2004).
URL
`http://www.theory.caltech.edu/~preskill/ph219/topological.ps`

[79] P. H. Bonderson, Non-Abelian Anyons and Interferometry, Ph.D. thesis (2007).

[80] L. Zehnder, Ein neuer Interferenzrefractor, Zeitschr. f. Instrkde. 11 (1891) 275–285.

[81] L. Mach, Über einer Interferenzrefractor, Zeitschr. f. Instrkde. 12 (1892) 89–93.

[82] P. Bonderson, K. Shtengel, J. K. Slingerland, Decoherence of anyonic charge in interferometry measurements, Phys. Rev. Lett. 98 (2007) 070401, quant-ph/0608119.

[83] B. J. Overbosch, F. A. Bais, Inequivalent classes of interference experiments with non-Abelian anyons, Phys. Rev. A 64 (2001) 062107, quant-ph/0105015.

[84] A. Zeilinger, General properties of lossless beam splitters in interferometry, Am. J. Phys. 49 (1981) 882–883.

[85] P. Bonderson, K. Shtengel, J. K. Slingerland, Probing non-Abelian statistics with quasiparticle interferometry, Phys. Rev. Lett. 97 (2006) 016401, cond-mat/0601242.

[86] M. H. Freedman, M. J. Larsen, Z. Wang, The two-eigenvalue problem and density of Jones representation of braid groups, Commun. Math. Phys. 228 (2002) 177–199, math/0103200.

[87] Y. Ji, Y. Chung, D. Sprinzak, M. Heiblum, D. Mahalu, H. Shtrikman, An electronic Mach–Zehnder interferometer, Nature 422 (2003) 415–418, cond-mat/0303553.

[88] I. Neder, M. Heiblum, Y. Levinson, D. Mahalu, V. Umansky, Coherence and phase in an electronic Mach–Zehnder interferometer: An unexpected behavior of interfering electrons (2005), cond-mat/0508024.

[89] I. Neder, M. Heiblum, Y. Levinson, D. Mahalu, V. Umansky, Unexpected behavior in a two-path electron interferometer, Phys. Rev. Lett. 96 (2006) 016804.

[90] C. L. Kane, Telegraph noise and fractional statistics in the quantum Hall effect, Phys. Rev. Lett. 90 (2003) 226802, cond-mat/0210621.

[91] T. Jonckheere, P. Devillard, A. Crepieux, T. Martin, Electronic Mach–Zehnder interferometer in the fractional quantum Hall effect, Phys. Rev. B 72 (2005) 201305(R), cond-mat/0503617.

[92] K. T. Law, D. E. Feldman, Y. Gefen, Electronic Mach-Zehnder interferometer as a tool to probe fractional statistics, Phys. Rev. B 74 (2006) 045319, cond-mat/0506302.

[93] D. E. Feldman, A. Kitaev, Detecting non-Abelian statistics with an electronic Mach–Zehnder interferometer, Phys. Rev. Lett. 97 (2006) 186803, cond-mat/0607541.

[94] C. Fabry, A. Pérot, Sur les franges des lames minces argenteés et leur application à la mesure de petites épaisseurs d'air, Ann. Chim. Phys. 12 (1897) 459–501.

[95] C. de C. Chamon, D. E. Freed, S. A. Kivelson, S. L. Sondhi, X. G. Wen, Two point-contact interferometer for quantum Hall systems, Phys. Rev. B 55 (1997) 2331–43, cond-mat/9607195.

[96] E. Fradkin, C. Nayak, A. Tsvelik, F. Wilczek, A Chern-Simons effective field theory for the Pfaffian quantum Hall state, Nucl. Phys. B 516 (1998) 704–18, cond-mat/9711087.

[97] A. Stern, B. I. Halperin, Proposed experiments to probe the non-abelian $\nu = 5/2$ quantum Hall state, Phys. Rev. Lett. 96 (2006) 016802, cond-mat/0508447.

[98] P. Bonderson, A. Kitaev, K. Shtengel, Detecting non-Abelian statistics in the $\nu = 5/2$ fractional quantum Hall state, Phys. Rev. Lett. 96 (2006) 016803, cond-mat/0508616.

[99] E. Grosfeld, S. H. Simon, A. Stern, Switching noise as a probe of statistics in the fractional quantum Hall effect, Phys. Rev. Lett. 96 (2006) 226803, cond-mat/0602634.

[100] C.-Y. Hou, C. Chamon, "Wormhole" geometry for entrapping topologically protected qubits in non-Abelian quantum Hall states and probing them with voltage and noise measurements, Phys. Rev. Lett. 97 (2006) 146802, cond-mat/0603142.

[101] P. Fendley, M. P. A. Fisher, C. Nayak, Dynamical disentanglement across a point contact in a non-Abelian quantum Hall state, Phys. Rev. Lett. 97 (2006) 036801, cond-mat/0604064.

[102] P. Fendley, M. P. A. Fisher, C. Nayak, Edge states and tunneling of non-Abelian quasiparticles in the $\nu = 5/2$ quantum Hall state and p+ip superconductors, Phys. Rev. B 75 (2007) 045317, cond-mat/0607431.

[103] E. Ardonne, E.-A. Kim, Hearing non-abelian statistics from a Moore–Read double point contact interferometer (2007), arXiv:0705.2902.

[104] B. J. Overbosch, X.-G. Wen, Dynamical and scaling properties of $\nu = 5/2$ interferometer (2007), arXiv:0706.4339.

[105] S. B. Chung, M. Stone, Proposal for reading out anyon qubits in non-Abelian $\nu = 12/5$ quantum Hall state, Phys. Rev. B 73 (2006) 245311, cond-mat/0601594.

[106] L. Fidkowski, Double point contact in the k=3 Read–Rezayi state (2007), arXiv:0704.3291.

[107] E.-A. Kim, Aharanov–Bohm interference and fractional statistics in a quantum Hall interferometer, Phys. Rev. Lett. 97 (2006) 216404, cond-mat/0604359.

[108] B. Rosenow, B. I. Halperin, Influence of interactions on flux and back-gate period of quantum Hall interferometers, Phys. Rev. Lett. 98 (2007) 106801, cond-mat/0611101.

[109] D. J. Thouless, Y. Gefen, Fractional quantum Hall effect and multiple Aharonov–Bohm periods, Phys. Rev. Lett. 66 (1991) 806–809.

[110] J. B. Miller, I. P. Radu, D. M. Zumbuhl, E. M. Levenson-Falk, M. A. Kastner, C. M. Marcus, L. N. Pfeiffer, K. W. West, Fractional quantum Hall effect in a quantum point contact at filling fraction 5/2 (2007), cond-mat/0703161.

[111] X. G. Wen, A. Zee, Classification of Abelian quantum Hall states and matrix formulation of topological fluids, Phys. Rev. B 46 (1992) 2290–301.

[112] R. B. Laughlin, Anomalous quantum Hall effect: an incompressible quantum fluid with fractionally charged excitations, Phys. Rev. Lett. 50 (1983) 1395–8.

[113] F. D. M. Haldane, Fractional quantization of the Hall effect: A hierarchy of incompressible quantum fluid states, Phys. Rev. Lett. 51 (1983) 605–608.

[114] B. I. Halperin, Statistics of quasiparticles and the hierarchy of fractional quantized Hall states, Phys. Rev. Lett. 52 (1984) 1583–6.

[115] J. K. Jain, Composite fermion approach for the fractional quantum Hall effect, Phys. Rev. Lett. 63 (1989) 199–202.